Classification of magnons in rotated ferromagnetic Heisenberg model and their competing responses in transverse fields

Fadi Sun,[1,2,3] Jinwu Ye,[1,3,4] and Wu-Ming Liu[2]

[1]*Department of Physics, Capital Normal University, Key Laboratory of Terahertz Optoelectronics, Ministry of Education, and Beijing Advanced innovation Center for Imaging Technology, Beijing 100048, China*

[2]*Beijing National Laboratory for Condensed Matter Physics, Institute of Physics, Chinese Academy of Sciences, Beijing 100190, China*

[3]*Department of Physics and Astronomy, Mississippi State University, Mississippi 39762, USA*

[4]*Kavli Institute of Theoretical Physics, University of California, Santa Barbara, Santa Barbara, California 93106, USA*

(Received 20 January 2016; revised manuscript received 27 May 2016; published 7 July 2016)

In this paper, we study the rotated ferromagnetic Heisenberg model (RFHM) in two different transverse fields, h_x and h_z, which can be intuitively visualized as studying spin-orbit coupling (SOC) effects in two-dimensional (2D) Ising or anisotropic XY model in a transverse field. At a special SOC class, it was found in our previous work [Phys. Rev. A **92**, 043609 (2015)] that the RFHM at a zero field owns an exact spin-orbit coupled ground state called the Y-x state. It supports not only the commensurate magnons (called C-C_0 and C-C_π), but also the incommensurate magnons (called C-IC). These magnons are nonrelativistic, not embedded in the exact ground state, so need to be thermally excited or generated by various external probes. Their dramatic response under a longitudinal h_y field was recently worked out by Sun *et al.* [arXiv:1502.05338]. Here we find they respond very differently under the two transverse fields. Any h_x (h_z) introduces quantum fluctuations to the ground state and changes the collinear Y-x state to a canted coplanar YX-x (YZ-x) state. The C-C_0, C-C_π, and C-IC magnons become relativistic and sneak into the quantum ground state. We determine the competing boundaries among the C-C_0, C-C_π, and C-IC magnons, especially the detailed dispersions of the C-IC magnons inside the canted phases, which can be mapped out by the transverse spin structure factors. As h_x (h_z) increases further, the C-C_0 magnons always win the competition and emerge as the seeds to drive a transition from the YX-x (or YZ-x) to the ferromagnetic along the X (or$Z$) direction called the X-FM (or Z-FM) phase. We show that the transition is in the 3D Ising universality class and it becomes the 3D XY transition at the two Abelian points. We evaluate these magnons' contributions to magnetization and specific heat at low temperatures which can be measured by various established experimental techniques. The nature of the finite-temperature transitions are also studied. Some analogies with quantum fluctuations generated multiple vortices and multiple landscapes in quantum spin glass are mentioned. The implications to cold-atom systems and some 4d and 5d materials with strong SOC are briefly discussed.

DOI: 10.1103/PhysRevB.94.024409

I. INTRODUCTION

A fundamental problem in any branch of physics regards the nature of the ground state. In strongly correlated electron systems, competing orders comprise a general concept to describe various quantum phases and transitions in various materials [1–6]. In this work, we focus on competing excitations in a given quantum phase which could lead to a natural explanation of some competing orders. It is known that a given quantum phase can still support different kinds of excitations with their own characteristics. These different classes of excitations are generated by quantum fluctuations inherent in the quantum ground state, so are intrinsic objects embedded in the ground state itself. Under various external probes; these excitations compete to emerge to drive the instability of the system into various other quantum phases through different universality classes of quantum phase transitions. So classifying different classes of excitations of a given phase and investigating their behaviors under various external probes could lead to deep understandings not only on the nature of the ground state itself, but also its broad connections to various other quantum phases.

A quantum phase is characterized by its symmetry breaking and excitation spectrum [1–6]. For quantum spin or bosonic systems, gapless excitations indicate long-range correlations encoded in the quantum phase. External probes could open a positive gap to the excitation or induce a "negative" gap, which indicates a quantum phase transition to another phase, while gapped excitations indicate short-ranged fluctuations encoded in the phase. The external probes such as magnetic fields, pressures, electric fields, etc., may drive these gapped excitations near a QCP, close their gaps, and lead to their condensations into a new phase through a quantum phase transition. For fermionic systems [7–13], the quantum phase supports both fermionic excitation and collective bosonic excitations. The two sectors may compete to lead to various other quantum phases under various external probes. Due to the absence of any symmetry breaking, a topological phase (such as quantum Hall state, spin liquids, etc.) [4,6,7] is characterized by its topological orders and associated fractionalized excitations. The gap closings of these fractionalized excitations could lead to another topological phase through a topological phase transition. In this work, we only focus on quantum phases without topological orders and with only different kinds of bosonic excitations.

In a previous work [14], the authors studied interacting spinor bosons at integer fillings hopping in a square optical lattice subject to any linear combinations of Rashba and Dresselhaus spin-orbit coupling (SOC). In the strong-coupling

limit, it leads to the rotated ferromagnetic Heisenberg model (RFHM) [Eq. (1)] at a zero Zeeman field [15–17], which is a new class of quantum spin models to describe quantum magnetisms in cold-atom systems or some materials with strong SOC. The RFHM [14] with any spin S at a generic SOC parameters (α,β) in a square lattice in a Zeeman field $\vec{H}$ is described by

$$\mathcal{H} = -J\sum_i [\mathbf{S}_i R_x(2\alpha)\mathbf{S}_{i+x} + \mathbf{S}_i R_y(2\beta)\mathbf{S}_{i+y}] - \vec{H}\cdot\sum_i \vec{S}, \quad (1)$$

where $J>0$ is the ferromagnetic interaction and the sum is over a unit cell i in a square lattice and the $R_x(2\alpha)$, $R_y(2\beta)$ are the two SO(3) rotation matrices around $\hat{x}$, $\hat{y}$ spin axis by the angle $2\alpha, 2\beta$, which are put on the two bonds $\hat{x}$, $\hat{y}$, respectively. As shown in [14], at $H=0$, the Hamiltonian Eq. (1) has the time-reversal ($\mathcal{T}$) symmetry, translational symmetry and three spin-orbital coupled Z_2 symmetries $\mathcal{P}_x,\mathcal{P}_y,\mathcal{P}_z$: (1) $\mathcal{P}_x$ symmetry, $S^x\to S^x$, $k_y\to -k_y$, $S^y\to -S^y$, $S^z\to -S^z$; (2) $\mathcal{P}_y$ symmetry, $S^y\to S^y$, $k_x\to -k_x$, $S^x\to -S^x, S^z\to -S^z$; (3) $\mathcal{P}_z$ symmetry, $k_x\to -k_x$, $S^x\to -S^x$, $k_y\to -k_y$, $S^y\to -S^y$, $S^z\to S^z$, which is also equivalent to a joint π rotation of the spin and orbital around $\hat{z}$ axis. Along the line $(\alpha=\pi/2,\beta)$, it also has the spin-orbital coupled $\mathrm{U(1)_{soc}}$ symmetry $[H,\sum_i(-1)^{i_x}S_i^y]=0$. Under the local rotation $\tilde{\mathbf{S}}_i = R_x(\pi)R_y(i_y\pi)\mathbf{S}_i$ followed by the $\mathcal{T}$, which is called mirror transformation $\mathcal{M}$ in [18], $\beta\to\pi/2-\beta$. At the middle point, $\beta=\pi/4$, the Hamiltonian is invariant under such a mirror transformation.

At the two Abelian points $\beta=0,\pi/2$ and $H=0$ in Eq. (1), the Hamiltonian has the SU(2) symmetry in the rotated basis $\tilde{\mathrm{SU}}(2)$ with $\tilde{\mathbf{S}}_i = R_x(i_x\pi)\mathbf{S}_i$ or $\tilde{\tilde{\mathrm{SU}}}(2)$ with $\tilde{\tilde{\mathbf{S}}}_i = R_x(i_x\pi)R_y(i_y\pi)\mathbf{S}_i$, respectively. Transferring back to the original basis, the SU(2) symmetry is generated by $\sum_i S_i^x$, $\sum_i(-1)^{i_x}S_i^y$, $\sum_i(-1)^{i_x}S_i^z$ at $\beta=0$ and by $\sum_i(-1)^{i_y}S_i^x$, $\sum_i(-1)^{i_x}S_i^y$, $\sum_i(-1)^{i_x+i_y}S_i^z$ at $\beta=\pi/2$, respectively. Both contain $\sum_i(-1)^{i_x}S_i^y$. At any h_y studied in [18], only $\sum_i(-1)^{i_x}S_i^y$ remains as a conserved quantity at both $\beta=0$ and $\beta=\pi/2$. In fact, as mentioned above [14], the spin-orbital coupled $\mathrm{U(1)_{soc}}$ symmetry $[H,\sum_i(-1)^{i_x}S_i^y]=0$ extends along the whole line $(\alpha=\pi/2,\beta)$ at any h_y.

At any $h_x\neq 0$, only $\sum_i S_i^x$ and $\sum_i(-1)^{i_y}S_i^x$ remains as a conserved quantity at $\beta=0$ and $\beta=\pi/2$, respectively. At any $h_z\neq 0$, only $\sum_i(-1)^{i_x}S_i^z$ and $\sum_i(-1)^{i_x+i_y}S_i^z$ remain as conserved quantities at $\beta=0$ and $\beta=\pi/2$, respectively. So the U(1) symmetry at the two Abelian points $\beta=0,\pi/2$ at a nonzero h_x,h_z is very much different than the $\mathrm{U(1)_{soc}}$ symmetry along the line $(\alpha=\pi/2,\beta)$ at $h_x=0$ or $h_z=0$ case. This distinction is important in the following two sections, Secs. I and II.

When expanding [14] the two R matrices in Eq. (1), it leads to a Heisenberg [1,2] + ferromagnetic Kitaev [19] (or quantum compass in a square lattice) + Dzyaloshinskii-Moriya (DM) interaction [20,21]. For a specific SOC class, we identify a spin-orbital entangled commensurate ground state: the Y-x state shown at the horizontal axis in Figs. 1 and 5. It supports three kinds of magnons: commensurate magnons such as C-C_0 and C-C_π and also a new gapped elementary excitation, incommensurate magnon (C-IC), with its two gap minima continuously tuned by the SOC strength. They are gapped bosonic excitations taking nonrelativistic dispersion with anisotropic effective mass m_x, m_y. However, the Y-x ground state is an exact quantum ground state with no quantum fluctuations. So the C-C_0, C-C_π, C-IC magnons in the RFHM are extrinsic, not embedded in the ground state due to the absence of quantum fluctuations. They need to be excited by thermal fluctuations or dragged out by various external probes which introduce quantum fluctuations into the ground state. Their parameters such as the minimum positions $(0,\pm k_y^0)$, gap Δ, and masses m_x, m_y can only be measured by various characteristics of the transverse structure factor at a finite T: It is a Gaussian shape, peaked at $(0,\pm k_y^0)$ with an exponentially suppressed amplitude $e^{-\Delta/T}$, with a temperature-dependent width $\sigma_x=\sqrt{m_x(\beta)T}$. The existence of the C-IC above a commensurate phase is the most striking feature of the RFHM. An important question to ask is how to drag out these magnons by various external probes, closing their gaps, and drive into new quantum phases through the condensation of these magnons.

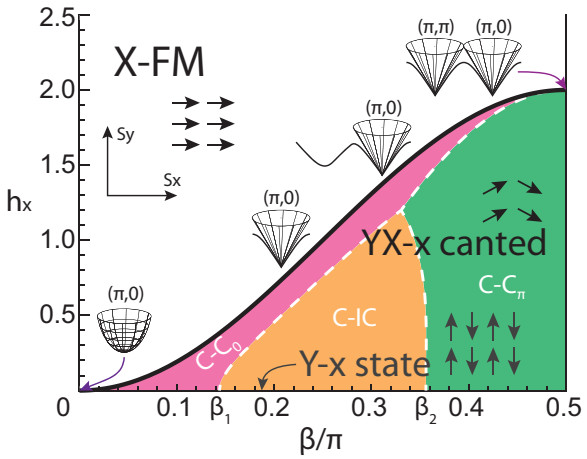

FIG. 1. Phase diagram of the RFHM in a transverse field h_x. Boundaries between C-C_0, C-C_π, and C-IC are indicated by white dashed lines. At $h_x=0$, the boundary between C-C_0 and C-IC is β_1 and that between C-C_π and C-IC is β_2, as shown in Ref. [14]. They are nonrelativistic. At $h_x=0$, the ground state is the Y-x state which is exact without any quantum fluctuations. So it contains no information of C-C_0, C-C_π, and C-IC. Any $h_x>0$ introduces quantum fluctuations and transfers them into the YX-x canted state. The C-C_0, C-C_π, and C-IC sneak into the YX-x ground state and become relativistic. At the critical field $h_c(\beta)$, the YX-x canted state undergoes a quantum phase transition to the X-FM state. It is in the 3D Ising university class and always driven by the condensation of C-C_0 magnons. The C-IC and C-C_π magnons always lose to the C-C_0 magnons before hitting the phase boundary. However, at the Abelian point $\beta=\pi/2$, C-C_0 and C-C_π magnons condense simultaneously and lead to a 3D XY class transition to the X-FM. The fine landscape of the C-IC regime is given in Fig. 2 and also discussed in detail in Appendix B. As shown in [13,14], the dispersions of C-C_0, C-C_π, and C-IC magnons can be mapped out by the transverse spin structure factors.

In a recent work [18], the authors showed that applying a uniform longitudinal Zeeman field h_y could do the job very well: The C-C_0, C-C_π, C-IC magnons compete to emerge under its effects to drive quantum phase transitions. It turns out that the C-IC always win the competition. Indeed, any infinitesimal small Zeeman field h_y immediately drags out the C-IC magnon and drives the condensation of the C-IC at $h = h_{c1}$, which vanishes as $\beta \to 0, \pi/2$; therefore, the Y-x state to noncoplanar incommensurate Skyrmion crystal (IC-SkX) phases through new universality class of quantum phase transitions. The IC-SkX phase is strikingly similar to the incommensurate, counter-rotating (in A/B sublattice), noncoplanar magnetic orders detected on iridates [22–24] α,β,γ-Li_2IrO_3.

Because the SOC breaks the spin rotation symmetry, the two transverse fields h_x, h_z may play quite different roles in dragging out the C-IC magnons and therefore drive into completely different phases and phase transitions than the longitudinal field h_y studied in [18]. These are the goals to be studied in this paper. Following [14,18], in this work, we also focus along the solvable line $(\alpha = \pi/2, \beta)$ of the RFHM in a transverse field [Eqs. (2) and (30)]. Results away from $\alpha = \pi/2$ will be briefly mentioned in the Conclusion section and be presented in a separate publication. The two models can be considered as incorporating possible dramatic effects of SOC on a well-studied two-dimensional (2D) Ising, anisotropic (or isotropic) quantum XY model in a transverse field [5]. They are also complimentary to the previous study of frustrated Ising model in a transverse field [25,26]. Note that the h_y field in [18] keeps the $U(1)_{soc}$ symmetry $\sum_i (-1)^x S_i^y$ of the Hamiltonian at the zero field, but h_x, h_z breaks it. This fact alone may lead to dramatic different competition among the magnons when they are subject to the longitudinal h_y or the two transverse fields h_x and h_z. Indeed, in the longitudinal field h_y, under the mirror transformation [18], $(\beta, h_y) \to (\pi/2 - \beta, h_y)$. So $\beta = \pi/4$ still enjoys the mirror symmetry. However, because h_x and h_z explicitly break the U(1) symmetry, the mirror transformation does not work anymore in the h_x and h_z cases. However, in the h_x case, we are still able to find a generalized mirror transformation to characterize systematically the competitions among the magnons on the two sides of $\beta = \pi/4$. Unfortunately, there is even no such a generalized mirror transformation in the h_z case, so the competitions are more intricate in the h_z field than in h_x field. The main results achieved in the h_x and h_z case are summarized in the beginning of Secs. II and III. Their relations to some previous works are given in Sec. IV.

Very recently, there was a remarkable experimental realization of 2D Rashba or Dresselhaus SOC or any of their linear combinations in Fermi gas or spinor Bose-Einstein condensate [27,28] in a square lattice. Various Zeeman fields are naturally generated by the Raman lasers. The two models Eqs. (2) and (30) can be realized in these cold-atom experiments. The results achieved in this work can be detected by various techniques such as specific heat [29,30], *in situ* measurement [31], and light or atom Bragg spectroscopy [32,33]. They may also shed some light on the study of magnetic orderings in some strongly correlated SOC materials [7,18,22–24], such as α,β,γ-Li_2IrO_3, with h_x, h_z playing the roles of different crystal fields or external applied magnetic fields.

II. TRANSVERSE FIELD h_x

In this section, we study the RFHM at $(\alpha = \pi/2, \beta)$ [Eq. (1)] in the h_x field:

$$\mathcal{H} = -J \sum_i [\mathbf{S}_i R_x(\pi) \mathbf{S}_{i+x} + \mathbf{S}_i R_y(2\beta) \mathbf{S}_{i+y}] - H_x \sum_i S_i^x . \tag{2}$$

Any H_x will break all the symmetries of the Hamiltonian at $H_x = 0$, except the $\mathcal{P}_x$ symmetry. It also keeps the combined $\mathcal{T}\mathcal{P}_y$ and $\mathcal{T}\mathcal{P}_z$ symmetries.

The main results to be achieved in this section are summarized as follows: In the h_x field, any infinitesimal h_x will change the Y-x state into a canted YX-x state (Fig. 1). In sharp contrast to the Y-x state, which is an exact ground state free of quantum fluctuations, the YX-x state suffers quantum fluctuations. So at $T = 0$, these magnons are quantum fluctuations generated, sneak into the YX-x state and become important components embedded inside the quantum ground state. They stand for quantum fluctuations with intrinsic wavelength and frequency and so can be detected by spin structure factor even at $T = 0$. We also evaluate their contributions to magnetization, specific heat, and uniform and staggered longitudinal susceptibilities at a finite temperature. Using the generalized mirror transformation, we map out the competing boundaries of the commensurate magnons C-C_0 and C-C_π and the incommensurate magnons C-IC inside the YX-x canted phase shown in Figs. 1 and 2. As h_x increases, the C-C_0 magnons emerge from the competitions and drives

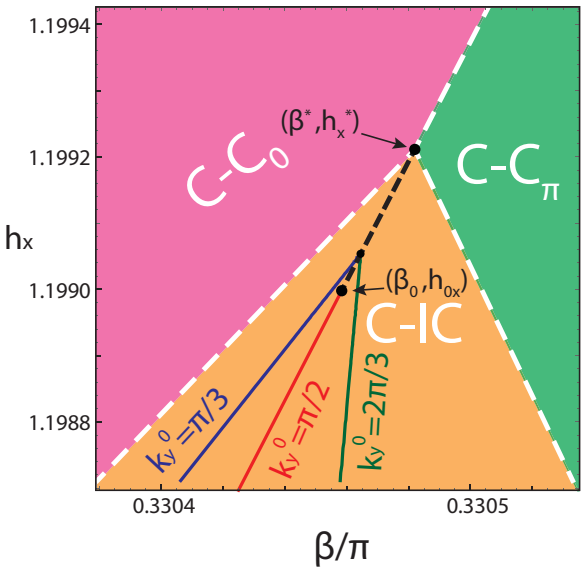

FIG. 2. The evolution of the C-IC magnons and the boundaries of the three kinds of magnons in Fig. 1 magnified ($\times 10^4$) around ($\beta_0 = 0.330\,458\pi$, $h_{0x} = 1.198\,99$) and ($\beta^* = 0.330\,482\pi$, $h_x^* = 1.199\,21$). There is a generalized mirror symmetry around $k_y^0 = \pm\pi/2$. The minimum at $(0, \pm k_y^0)$ and its mirror image at $[0, \pm(\pi - k_y^0)]$ symmetrically located on the two sides of $k_y^0 = \pm\pi/2$ must end in the regime $\beta_0 < \beta < \beta^*$, where they become degenerate minima. The three segments of the contour line $k_y^0 = \pm\pi/2$ are explained in the text and also Appendix B. As shown in [13,14], the C-IC dispersion can be mapped out by the transverse spin structure factors.

the quantum phase transition at a critical field $h_{cx}(\beta)$ from the YX-x phase to the ferromagnetic X-FM phase in Fig. 1. By performing symmetry analysis, identifying a suitable order parameter and contrasting with the spin-wave expansion, we find it is in the 3D Ising universality class. Due to the enlarged U(1) symmetry mentioned in the Sec. I, the transition at the Abelian $\beta = \pi/2$ point is driven by the simultaneous condensations of the C-C_0 and C-C_π magnons and is in the universality class of the 3D XY model. We also work out the finite-temperature phase diagram in Fig. 4.

A. X-FM state and excitations in a high field

To map out the phases of Eq. (2), it is instructive to start from the high field limit $H_x \gg J$. In this limit, the system is in X-FM phase with all the spins fully (classically) polarized to S_x direction (Fig. 1). Obviously, the X-FM keeps all the symmetries of the Hamiltonian.

Under the global spin rotation $(S_i^x, S_i^y, S_i^z) \to (S_i^z, S_i^y, -S_i^x)$, the Hamiltonian Eq. (2) becomes

$$\mathcal{H} = -J \sum_i [\mathbf{S}_i R_z(\pi) \mathbf{S}_{i+x} + \mathbf{S}_i R_y(2\beta) \mathbf{S}_{i+y}] - H_x \sum_i S_i^z. \tag{3}$$

Introducing the Holstein-Primakoff (HP) bosons [14,18], $S^+ = \sqrt{2S - a^\dagger a}\, a$, $S^- = a^\dagger \sqrt{2S - a^\dagger a}$, $S^z = S - a^\dagger a$, the Hamiltonian Eq. (3) can be written in a systematic $1/S$ expansion in terms of the HP bosons. Up to the linear spin-wave (LSW) order at $1/S$, we get

$$\mathcal{H}_2 = E_0 + 2JS \sum_k \{[h_x + \cos k_x + \cos^2\beta(2 - \cos k_y)] a_k^\dagger a_k + \sin^2\beta \cos k_y (a_k a_{-k} + a_k^\dagger a_{-k}^\dagger)/2\}, \tag{4}$$

where the classical ground-state energy $E_0 = -2JNS^2 \cos^2\beta - H_x NS$ and we have introduced the dimensionless field $h_x = H_x/(2JS)$. Now the Hamiltonian can be diagonalized by a Bogoliubov transformation,

$$\mathcal{H}_2 = E_0' + 4JS \sum_k \omega_k \alpha_k^\dagger \alpha_k, \tag{5}$$

where the ground-state energy at the order of $1/S$ is $E_0' = E_0 - 2JS \sum_k \omega_k$ and the energy spectrum is

$$\omega_k = \sqrt{[h_x + \cos k_x + \cos^2\beta(2 - \cos k_y)]^2 - \sin^4\beta \cos^2 k_y}, \tag{6}$$

where, for $0 < \beta < \pi/2$, one can identify that there is a unique minimum located at $k^0 = (k_x, k_y) = (\pi, 0)$ with the energy gap

$$\Delta_\pi = \omega_{k=k^0} = \sqrt{h_x(h_x - 1 + \cos 2\beta)}. \tag{7}$$

The gap vanishing condition leads to the critical field strength h_c,

$$h_{cx}(\beta) = 1 - \cos 2\beta = 2\sin^2\beta, \tag{8}$$

which is shown in Fig. 1. The gap vanishing at $k^0 = (k_x, k_y) = (\pi, 0)$ indicate a quantum phase transition into a spin-orbital correlated state with orbital order $(\pi, 0)$. It was known that at $h_x = 0$, the ground state Y-x state also has the $(\pi, 0)$ orbital order. That indicates that there is only one phase transition and the state below h_{cx} could be just the YX-x state with a canted angle. As to be shown in the next section, we show that it is indeed the YX-x state with the orbital order $(\pi, 0)$. So near the Quantum Phase transition (QPT), $\Delta_\pi \sim (h_x - h_{cx})^{1/2}$.

From Eq. (6), we find the excitation spectrum around the minimum $k^0 = (\pi, 0)$ takes the relativistic form

$$\omega_q = \sqrt{\Delta_\pi^2 + v_x^2 q_x^2 + v_y^2 q_y^2}, \quad k = k^0 + q, \tag{9}$$

where

$$v_x^2 = (2h_x - 1 + \cos 2\beta)/2, \qquad v_y^2 = [h_x + \cos 2\beta(h_x - 1 + \cos 2\beta)]/2. \tag{10}$$

At $h = h_{cx}$, $\Delta_\pi = 0$, the critical velocities are $v_{x,c}^2 = v_{y,c}^2 = \sin^2\beta$. As long as $\beta > 0$, we obtain a nonzero critical velocity, which indicates a relativistic critical behavior with the dynamic exponent $z = 1$.

Before starting the next section, we discuss a little bit further the enlarged symmetry and its consequences at the two Abelian points $\beta = 0, \pi/2$ in Fig. 1.

The $U(1)$ symmetry at the two Abelian points $\beta = 0, \pi/2$ at a nonzero field h_x

At the two Abelian points $\beta = 0, \pi/2$ and $h_x = 0$, the system has a SU(2) symmetry in the rotated basis $\tilde{\text{SU}}(2)$, with $\tilde{\mathbf{S}}_i = R_x(i_x\pi)\mathbf{S}_i$ or $\tilde{\tilde{\text{SU}}}(2)$ with $\tilde{\tilde{\mathbf{S}}}_i = R_x(i_x\pi)R_y(i_y\pi)\mathbf{S}_i$, respectively. So Eq. (2) can be mapped to a FM Heisenberg model in $-h_x \sum_i \tilde{S}_i^x$ and $-h_x \sum_i (-1)^{i_y} \tilde{\tilde{S}}_i^x$ [see Eq. (11)], respectively. So at $\beta = 0$, any h_x will pick up the X-FM phase as the exact ground state. At $\beta = \pi/2$, taking the result from [18], any h_x will lead to a spin-flop transition, resulting in a U(1) symmetry-breaking canted phase with one Goldstone mode ϕ. Then there is another transition to the X-FM at a finite $h_c = 2$. These results at the two Abelian points fit into the general result Eq. (8) and shown in Fig. 1.

At $\beta = 0, h_x = 0$, transferring back to the original basis, the Hamiltonian Eq. (2) has the SU(2) symmetry generated by $\sum_i S_i^x$, $\sum_i (-1)^{i_x} S_i^y$, $\sum_i (-1)^{i_x} S_i^z$. At any $h_x > 0$, only $\sum_i S_i^x$ remains as a conserved quantity. Obviously, the X-FM state keeps all symmetries of the Hamiltonian. Having the conserved quantity $e^{i\phi \sum_i (-1)^{i_y} S_i^x}$ which carries the momentum $(0, \pi)$, act on the the excitation (or eigenstate) at the minimum $(\pi, 0)$ in Eq. (9) changes nothing. So at $\beta = 0, h_x > 0$, the system has only one minima located at $(\pi, 0)$, as shown in the left axis in the Fig. 1.

Similarly, at $\beta = \pi/2$, $h_x = 0$, transferring back to the original basis, the Hamiltonian Eq. (2) has the SU(2) symmetry generated by $\sum_i (-1)^{i_y} S_i^x$, $\sum_i (-1)^{i_x} S_i^y$, $\sum_i (-1)^{i_x + i_y} S_i^z$. At any $h_x > 0$, only $\sum_i (-1)^{i_y} S_i^x$ which carries momentum $(0, \pi)$ remains as a conserved quantity. Having the conserved quantity $e^{i \sum_i (-1)^{i_y} S_i^x}$, which carries the momentum $(0, \pi)$, act on the excitation(or eigenstate) at the minimum $(\pi, 0)$ in Eq. (9), will generate another minimum (π, π), so at $\beta = \pi, h_x > 0$, the system has two minima [18] located at $(\pi, 0)$ and (π, π), as shown in the right axis in the Fig. 1.

As stressed in the Introduction, the U(1) symmetry $\sum_i S_i^x$ or $\sum_i (-1)^{i_y} S_i^x$ at the Abelian points $\beta = 0$ or $\beta = \pi/2$ at a nonzero transverse field h_x is different than the spin-orbital

coupled U(1) symmetry $\sum_i (-1)^{i_x} S_i^y$ along the line ($\alpha = \pi/2, \beta$) at $h_x = 0$ in the RFHM Eq. (1).

B. *YX-x* canted state below h_{cx}

1. *Classical YX-x canted phase at $h < h_{cx}$*

When $\beta = \pi/2$, in the $\tilde{\text{SU}}(2)$ basis $\tilde{\tilde{\mathbf{S}}}_i = R_x(i_x\pi)R_y(i_y\pi)\mathbf{S}_i$, the Hamiltonian Eq. (2) takes the form

$$\mathcal{H} = -J\sum_{\langle ij\rangle} \tilde{\tilde{\mathbf{S}}}_i \cdot \tilde{\tilde{\mathbf{S}}}_j - H_x \sum_i (-1)^{i_y} \tilde{\tilde{S}}_i^x. \tag{11}$$

When $0 < H_x < H_{xc}$, the classical state takes the form

$$\tilde{\tilde{\mathbf{S}}}_i = S((-1)^{i_y}\cos\theta, \sin\theta\cos\phi, \sin\theta\sin\phi), \tag{12}$$

where ϕ is nothing but the Goldstone mode due to the U(1) symmetry breaking. Reverting back to the original basis, we obtain

$$\mathbf{S}_i = S(\cos\theta, (-1)^{i_x}\sin\theta\cos\phi, (-1)^{i_x+i_y}\sin\theta\sin\phi). \tag{13}$$

Note that although we obtained Eqs. (12) and (13) at $\beta = \pi/2$, the same ansatz hold for $0 < \beta < \pi/2$ whose classical ground energy is

$$E_c = -2NJS^2(1 + h_x\cos\theta - \sin^2\beta\cos^2\theta - \cos^2\beta\sin^2\theta\sin^2\phi). \tag{14}$$

It is easy to see that any deviation from $\beta = \pi/2$ explicitly breaks the U(1) symmetry at $\beta = \pi/2$ listed in Sec. II A, and so picks up $\phi = 0$, opens the gap to the Goldstone mode [34], and leads to the *YX-x* canted state,

$$\mathbf{S}_i = S(\cos\theta, (-1)^{i_x}\sin\theta, 0), \tag{15}$$

which indeed has the $(\pi, 0)$ order as indicated from the magnon condensations from the *X*-FM studied in the Sec. II A.

Substituting $\phi = 0$ in Eq. (14) leads to the classical ground-state energy

$$E_c = -2NJS^2(1 + h_x\cos\theta - \sin^2\beta\cos^2\theta), \tag{16}$$

whose minimization leads to the canted angle

$$\cos\theta = \frac{h_x}{2\sin^2\beta} < 1, \quad \text{when} \quad h_x < h_{cx}, \tag{17}$$

which always has a solution as long as $h_x < h_{cx}$.

Only when $h = h_{cx}, \theta = 0$ does it become the *X*-FM phase. The fact that we achieved the same critical field h_{cx} from the *X*-FM state Eq. (8) above it and the *YX-x* state Eq. (17) below it indicates that there is only one phase transition with the critical field $h = h_{cx}$ shown in Fig. 1. Note that from above $h > h_{cx}$, we achieved it by the LSW at the order of $1/S$, while from below $h > h_{cx}$ we achieved it just by the classical ground-state energy minimization at $S = \infty$.

In sharp contrast, in the h_y case [18], there are two critical fields $h_{c1} < h_{c2}$; there is an intermediate IC-SkX phase between the two critical fields.

2. *Spin-wave analysis in the YX-x canted state*

Again performing the global spin rotation $(S_i^x, S_i^y, S_i^z) \to (S_i^z, S_i^y, -S_i^x)$, then applying the spin rotation $R_x(\theta)$ for the *A* sublattice and $R_x(-\theta)$ for the *B* sublattice lead to

$$\begin{aligned}\mathcal{H} =& -J\sum_{i\in A}[S_i R_z(\pi)S_{i+x} + S_i R_x(\theta)R_y(2\beta)R_x(-\theta)S_{i+y}] \\ & - J\sum_{i\in B}[S_i R_z(\pi)S_{i+x} + S_i R_x(-\theta)R_y(2\beta)R_x(\theta)S_{i+y}] \\ & - H_x\sum_{i\in A}\left[\sin\theta S_i^y + \cos\theta S_i^z\right] \\ & - H_x\sum_{i\in B}\left[-\sin\theta S_i^y + \cos\theta S_i^z\right].\end{aligned} \tag{18}$$

Introducing the HP bosons $S^+ = \sqrt{2S - a^\dagger a}\,a$, $S^- = a^\dagger\sqrt{2S - a^\dagger a}$, and $S^z = S - a^\dagger a$ for sublattice *A* and $S^+ = \sqrt{2S - b^\dagger b}\,b$, $S^- = b^\dagger\sqrt{2S - b^\dagger b}$, $S^z = S - b^\dagger b$ for sublattice *B*, the Hamiltonian Eq. (18) can be written in a systematic $1/S$ expansion in terms of the HP bosons. Up to the LSW order at $1/S$, we get

$$\begin{aligned}\mathcal{H}_2 =& E_c + 2JS\sum_k[(A_k + B_k)a_k^\dagger a_k + (A_k - B_k)b_k^\dagger b_k \\ & + C_k(a_k^\dagger b_k + b_k^\dagger a_k) + D_k(a_k a_{-k} + b_k b_{-k} + \text{H.c.})],\end{aligned} \tag{19}$$

where E_c is the classical ground-state energy Eq. (16) and

$$\begin{aligned}A_k &= 2 - (\cos^2\beta - \sin^2\beta\sin^2\theta)\cos k_y, \\ B_k &= \sin 2\beta\sin\theta\sin k_y, \\ C_k &= \cos k_x, \\ D_k &= \sin^2\beta\cos^2\theta\cos k_y.\end{aligned} \tag{20}$$

The Hamiltonian Eq. (19) can be diagonalized by a Bogoliubov transformation

$$\mathcal{H}_2 = E_c' + 4JS\sum_k(\omega_k^-\alpha_k^\dagger\alpha_k + \omega_k^+\beta_k^\dagger\beta_k), \tag{21}$$

where $E_c' = E_c - 2JS\sum_k(\omega_k^- + \omega_k^+)$ is the ground-state energy up to the order of $1/S$ and the energy spectra are

$$\omega_k^\pm = \sqrt{A_k^2 + B_k^2 + C_k^2 - D_k^2 \pm 2\sqrt{A_k^2(B_k^2 + C_k^2) - B_k^2 D_k^2}}, \tag{22}$$

from which one can determine the minimum positions.

We found there are three regimes inside the *YX-x* canted state: C-C_0 regime, C-IC regime, and C-C_π regime which, at $h_x = 0$, reduce to the three regimes identified in [14]. Among the three regimes, only the C-C_0 regime sits just below the transition line h_{cx}, so the transition from the *YX-x* state to the *X*-FM is driven by the condensations of the C-C_0 magnons only. Then we find that just below the phase boundary, the C-C_0 magnons take also the relativistic form around $k_0 = (0,0)$,

$$\omega_q = \sqrt{\Delta_0^2 + v_x^2 q_x^2 + v_y^2 q_y^2}, \quad k = q + k_0, \tag{23}$$

where

$$\Delta_0 = \sqrt{(1-\cos 2\beta)\left(1-\cos 2\beta-\frac{h_x^2}{2\sin^2\beta}\right)},$$

$$v_x^2 = 2\sin^2\beta - \left(\frac{h_x}{2\sin\beta}\right)^2,$$

$$v_y^2 = \left[2\sin^2\beta-\left(\frac{h_x}{2\sin\beta}\right)^2\right] \times\left[\cos 2\beta-\sin^2 2\beta+\frac{h_x^2}{4\sin^2\beta}+\frac{h_x^2\cos^2\beta}{\sin^2\beta}\right] +\left(\frac{h_x}{2\sin\beta}\right)^4\left[1+\frac{\sin^2 2\beta\left(1-\frac{h_x^2}{4\sin^4\beta}\right)}{2-\cos 2\beta-\left(\frac{h_x}{2\sin\beta}\right)^2}\right]. \quad (24)$$

At $h = h_{cx}$, the critical velocities are $v_{x,c}^2 = v_{y,c}^2 = \sin^2\beta$, which are the same as those achieved from X-FM from above the h_{cx} in Eq. (10). Near h_{cx}, $\Delta \sim (h_{cx}-h)^{1/2}$. Now we can check the consistence of the orbital orders on both sides of h_{cx}. The YX-x state has the orbital order $(\pi,0)$; the C-C_0 has the orbital order $(0,0) = (\pi,0)$ in the reduced Brillouin zone (RBZ). So its condensation on the top of YX-x could lead to the two orbital orders, either $(\pi,0)+(0,0) = (\pi,0)$ or $(\pi,0)+(\pi,0) = (0,0)$, in the extended Brillouin zone (EBZ). The $(0,0)$ order is nothing but that of the X-FM in Fig. 1.

The competition between C-C_0 and C-C_π gives the boundary between C-C_0 and C-C_π, where they become degenerate (see Appendix B),

$$h_{0\pi} = 2\sin\beta\sqrt{-\cos 2\beta} < h_{cx}, \quad (25)$$

where $\beta^* \sim 0.330\,482\pi < \beta < \pi/2$.

The competition between C-C_0 and C-IC is given by the condition: $\frac{\partial^2\omega_k^-}{\partial k_y^2}|_{k=(0,0)} = 0$. That between C-$C_\pi$ and C-IC is given by the condition: $\frac{\partial^2\omega_k^-}{\partial k_y^2}|_{k=(0,\pi)} = 0$. We find that the three boundaries (dashed lines) in Fig. 1 meet at the same point ($\beta^* = 0.330\,482\pi$, $h_x^* = 1.199\,21$). The fine structure near this point is shown in Fig. 2.

C. Evolution of the C-IC magnons inside the C-IC regime in Fig. 1: Generalized mirror symmetry about the contour $k_y^0 = \pm\pi/2$

In the longitudinal field h_y, which keeps the spin-orbital coupled U(1) symmetry [18], there is a mirror transformation relating (β,h_y) to $(\pi/2-\beta,h_y)$. So $\beta = \pi/4$ enjoys the mirror symmetry. However, because h_x and h_z explicitly breaks the U(1) symmetry, so the mirror transformation does not work anymore in h_x and h_z case. Even so, it would be important to first understand the minimum contour at $k_y^0 = \pm\pi/2$. In the h_x case, it seems there is a "generalized" mirror transformation relating the minimum at $(0,\pm k_y^0)$ to its associated mirror image at $[0,\pm(\pi-k_y^0)]$ as shown in Fig. 2, while the $k_y^0 = \pm\pi/2$ is the self-dual line which starts at $(\beta = \pi/4, h_x = 0)$. Unfortunately, in contrast to the h_y case, it is difficult to find the exact form of such a generalized mirror transformation in terms of (β,h_x). Its form in terms of the contour k_y^0 would be enough to analyze the structure of the C-IC regime in Fig. 2 at least to the order of $1/S$. However, as to be shown in the next section, there is no generalized mirror symmetry in the h_z case.

As shown in the Appendix B, the minimum contour $k_y^0 = \pm\pi/2$ can be determined by the equation

$$h_{\pi/2}(\beta) = 2\sin\beta\sqrt{-\cos 2\beta}, \quad (26)$$

where $0.25\pi < \beta < \beta_0 \approx 0.330\,458\pi$.

If comparing Eq. (26) with the C-C_0/C-C_π boundary Eq. (25), we find out they have the same form but different domains. In fact, one can extend Eq. (26) to the whole domain $0.25\pi < \beta < 0.50\pi$, where we have two special β: $\beta_0 \approx 0.330\,458\pi$ and $\beta_* \approx 0.330\,482\pi$. For $0.25\pi < \beta < \beta_0$, Eq. (26) describes the minimum contour $k_y^0 = \pi/2$ shown in Fig. 8, for $\beta_* < \beta < 0.50\pi$; it describes the C-$C_0$/C-$C_\pi$ boundary. What happens when $\beta_0 < \beta < \beta_*$ is shown in Fig. 9 and summarized below.

As shown in the Fig. 2, the constant contour line at $k_y^0 = \pi/2$ can be divided into three segments. (1) $\pi/4 < \beta < \beta_0 \sim 0.330\,458\pi$, $k_y^0 = \pm\pi/2$ is indeed a minimum as shown in Fig. 8. (2) $\beta_0 < \beta < \beta^* \sim 0.330\,482\pi$, $k_y^0 = \pm\pi/2$ becomes a local maximum, $k_y^0 = 0,\pi$ are also local maximum. There are four degenerate minima $(0,\pm k_y^0)$ and $[0,\pm(\pi-k_y^0)]$ symmetrically located on the two sides of $k_y^0 = \pm\pi/2$, as shown in Fig. 9. At β_0, the second derivatives of the spectrum at $k_y^0 = \pm\pi/2$ vanish. (3) $\beta^* < \beta < \pi/2$, C-C_0, and C-C_π become two degenerate minima, with $k_y^0 = \pm\pi/2$ being still the maximum as shown in Fig. 2. At β^*, the second derivatives of the spectrum at $k_y^0 = 0,\pi$ vanish.

So all the two mirror related minima $(0,\pm k_y^0)$ and $[0,\pm(\pi-k_y^0)]$ must end in the regime $\beta_0 < \beta < \beta^*$ shown in Fig. 2, where they become four degenerate minima.

D. The transition from the YX-x canted state to the X-FM at $T = 0$ and finite T

1. *The zero-temperature transitions: Symmetry breaking and order parameters*

The transition from the YX-x canted state to the X-FM is characterized by the order parameter $M_y(T=0) = \langle S^y\rangle$, which is staggered along x axis. As said at the beginning of Sec. II, the Hamiltonian Eq. (2) has $\mathcal{P}_x$ symmetry: $S^x \to S^x$, $k_y \to -k_y$, $S^y \to -S^y$, $S^z \to -S^z$ and the translational symmetry. The X-FM respects both symmetries, so $M_y(T=0) = 0$, but the YX-x states break both, but keep its combination $\mathcal{P}_x \times (x \to x+1)$ as shown in Appendix A, so $M_y(T=0) \neq 0$. Due to the spin-orbital locking, destroying the $M_y(T=0) = \langle S^y\rangle$ order will also restore the translational symmetry along x direction. As shown in Eqs. (9) and (23), there are relativistic gapped C-C_0 magnons on both sides, indicating the dynamic exponent $z = 1$. So we conclude that the transition is in the 3D Ising universality class. The renormalization group (RG) flow is controlled by a fixed point on the phase boundary shown in Fig. 3.

At $h_x = 0$, the Y-x collinear state is the exact eigenstate [14], so $M_y(T=0) = S$. The ground state itself contains no information on the C-C_0, C-C_π, and C-IC magnons. As shown in Sec. II B, any $h_x \neq 0$ transfers the Y-x state into the YX-x canted state and also introduces quantum fluctuations. The canted angle of the classical YX-x state is given in

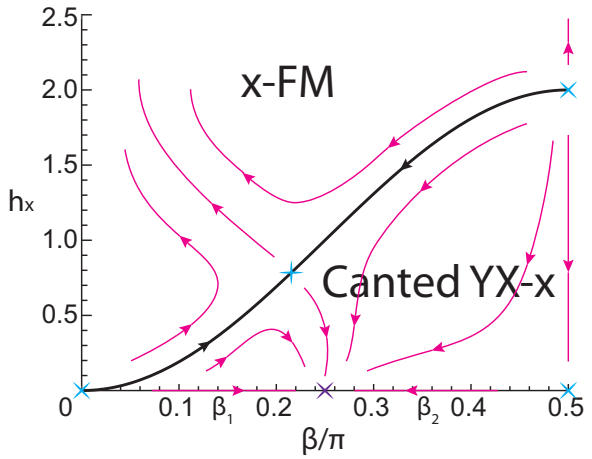

FIG. 3. The RG flow for RFHM in the transverse field h_x. There is a fixed point on the phase boundary controlling the zero-temperature transition from the YX-x state to the X-FM state, which is in the 3D Ising universality class. At the Abelian point $\beta = \pi/2$, the transition is in the 3D XY class. Any deviation from the two Abelian points are relevant and drive the system into the 3D Ising fixed point. All the crosses stand for RG fixed points. The whole YX-x state is controlled by the fixed point at ($\beta = \pi/4$,$h = 0$), which enjoys the enlarged mirror symmetry [14,18]. Inside the YX-x state, all the quantum fluctuation generated C-C_0, C-C_π, and C-IC are irrelevant under the RG sense, but they are the competing to become the driving seed to the X-FM. Figures 1 and 2 show that it is the C-C_0, which wins the competition and becomes the driving seed.

Eq. (17). The ground state itself contains information on the C-C_0, C-C_π, and C-IC magnons. They all compete and move to the phase transition boundary.

From the classical YX-x state Eq. (15) with the canted angle Eq. (17) and Eq. (19), we find that they reduce the order parameter below its classical value,

$$M_y(T=0) = M_c\left[1 - \frac{1}{2SN}\sum_k \left(\frac{P_k^+}{\omega_k^+} + \frac{P_k^-}{\omega_k^-} - 2\right)\right], \quad (27)$$

where $M_c = S\sqrt{1-(h/h_{cx})^2}$ is the classical order parameter and $P_k^\pm = A_k^2[1 \pm (B_k^2 + C_k^2)/\sqrt{A_k^2(B_k^2 + C_k^2) - B_k^2 D_k^2}]$.

When approaching the phase boundary $h_{cx} = 2\sin^2\beta$, the quantum fluctuations get stronger and stronger; finally, the C-C_0 wins the competition and the order parameter should vanish as $M_y(T=0) \sim (h_{cx} - h)^{\beta_{3d}}$ with the 3D Ising exponent $\beta_{\rm Ising} \sim 0.31$. Equation (27) leads to $M_y(T=0) \sim \Delta \sim (h_{cx} - h)^{1/2}$ with the mean-field exponent $\beta_{MF} = 1/2$. The quantum fluctuations at the LSW order do not change the phase boundary h_{cx} and the mean-field exponent. At the LSW order, near the critical line h_{cx}, the C-C_0 magnon gap Δ on both sides own the critical scaling $\Delta \sim |h - h_{cx}|^{1/2}$, which also gives the mean-field exponent $\nu_{MF} = 1/2$. Note that $\nu_{\rm Ising} = 0.64$ for the 3D Ising model. To achieve these exact 3D Ising exponents, one needs to incorporate the interactions between the magnons. In practice, just from the symmetry analysis, we conclude that the Ginsburg-Landau action to describe the transition is in the 3D Ising universality class. The $T = 0$ RG flow is shown in Fig. 3.

At the Abelian $\beta = \pi/2$ point, starting from $h > h_{cx}$, as shown in [18], due to the enlarged U(1) symmetry, the transition is driven by the simultaneous condensation of the magnons at the two degenerate minima $(\pi,0)$ and (π,π), from below $h < h_{cx}$, it is also a simultaneous condensations of C-C_0 and C-C_π magnons, so the transition is in the 3D XY universality class.

2. The low-temperature behaviors

Except at the Abelian point $\beta = 0$, $h = 0$, there is a gap $\Delta_-(\beta)$ in the excitation spectrum in the YX-x canted phase, so the order survives up to a finite critical temperature $T_{cx} \sim \Delta_-(\beta,h_x)$ above which the system gets to the X-FM state. Of course, at the phase boundary in Fig. 1, $\Delta_-(\beta,h_x) = 0$, so $T_{cx} = 0$. Note that the spin wave expansion works in the whole phase diagram in Fig. 1 at $T = 0$, but its use at a finite T is only limited to $T \ll T_{cx}$; it fails when getting too close to T_{cx}. At low temperatures $T < T_{cx}$, inside the C-IC regime in Fig. 1, by expanding ω_k^- in Eq. (22) around the C-IC minima $(0,\pm k_y^0)$, we find that the excitation spectrum takes the relativistic form

$$\omega_q = \sqrt{\Delta_{ic}^2 + v_x^2 q_x^2 + v_y^2 q_y^2}, \quad k = \left(0,\pm k_y^0\right) + q, \quad (28)$$

whose detailed behaviors along the $k_y^0 = \pm\pi/2$ are shown in Figs. 8 and 9. They dominate the contributions to the magnetization and the specific heat when $T \ll \Delta_{ic}$,

$$C_m(T) \sim \frac{\Delta_{ic}^3}{2\pi v_x v_y T} e^{-\Delta_{ic}/T},$$
$$M_y(T) \sim M_y(T=0) - \frac{T^2}{2\pi v_x v_y} e^{-\Delta_{ic}/T}, \quad (29)$$

where $M_y(T=0)$ is the zero-temperature staggered magnetization given in Eq. (27).

Following the procedures in [14], one can also evaluate the uniform and staggered susceptibilities along the y direction and various dynamic spin correlation functions. Especially, we expect that the C-IC magnons will lead to two split peaks located at $(0,\pm k_y^0)$ in the transverse spin structure factors $S^{+-}(\vec{k})$. All these physical quantities can be measured by specific heat [29,30], *in situ* measurement [31], and light or atom Bragg spectroscopy [32,33], respectively.

3. The finite-temperature phase transitions

Because inside the YX-x phase in Fig. 1, the RG flows to the fixed point ($\beta = \pi/4$, $h = 0$), so the finite-temperature transition from the YX-x canted phase to the X-FM is in the same universality class as that at the zero-field case. Its nature was briefly discussed in [14], where we argued that, due to the extra symmetry breaking of $\vec{\tilde{S}}_i = R_x(\pi)R_y(i_y\pi)\vec{S}_i$ at $\beta = \pi/4$, its universality class (Fig. 3 in [14]) remains to be determined. Here we argue that the universality class is simply a 2D Ising one with the order parameter $M_y = \langle S^y\rangle \neq 0$ in the low-temperature Y-x state and $M_y = 0$ in the high-temperature paramagnet (Fig. 3 in [14]). The extra symmetry breaking at $\beta = \pi/4$ should not affect its 2D Ising universality class. Of course, at the Abelian $\beta = \pi/2$ point, it is in the 2D XY universality class. The finite-temperature transitions at the Abelian point $\beta = \pi/2$, the mirror symmetric point $\beta = \pi/2$, and a given $0 < h_x < 2$ in Fig. 3 is shown in Fig. 4.

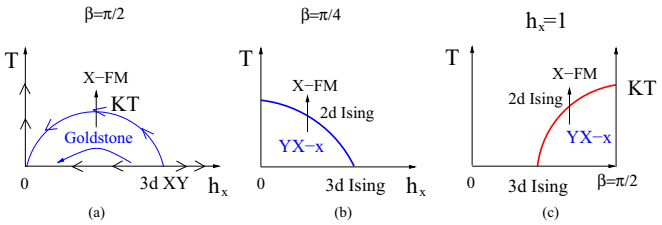

FIG. 4. Finite-temperature phase transitions. (a) At the Abelian point $\beta = \pi/2$. The arrows stand for the RG flow. Due to the U(1) symmetry breaking, there is a Goldstone mode and a 2D Kosterlitz-Thouless (KT) transition at the low-T phase. (b) T_c reaches maximum at the mirror symmetric non-Abelian point ($\beta = \pi/4$, $h_x = 0$) (see Fig. 3 in [14]). (c) At a fixed $0 < h_x < 2$. Shown is $h_x = 1$.

III. TRANSVERSE FIELD h_z

The RFHM in a transverse field along S_z direction is described by

$$\mathcal{H} = -J \sum_i [\mathbf{S}_i R_x(\pi) \mathbf{S}_{i+x} + \mathbf{S}_i R_y(2\beta) \mathbf{S}_{i+y}] - H_z \sum_i S_i^z, \tag{30}$$

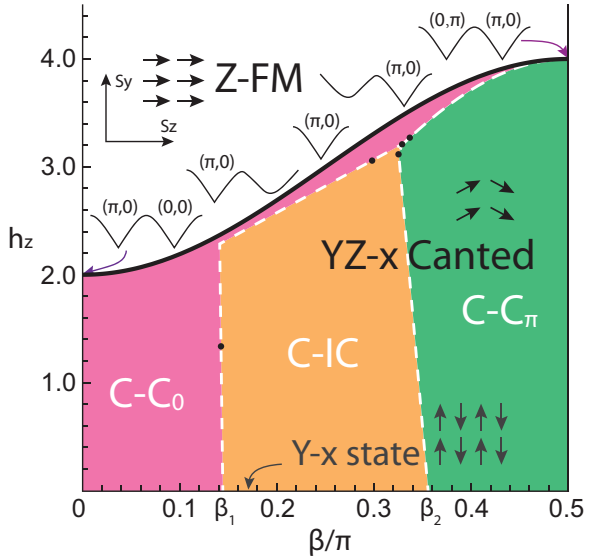

FIG. 5. Phase diagram for RFHM with transverse field h_z. Boundaries between C-C_0, C-C_π, and C-IC are indicated by white dashed lines. At $h_z = 0$, the ground state is the Y-x state, which is an exact without any quantum fluctuations. Any $h_z > 0$ will transfer it into the YZ-x canted state, which suffers quantum fluctuations. At the critical field $h_{cz}(\beta)$, the YZ-x canted state undergoes a quantum phase transition to the Z-FM state. It is in the 3D Ising university class and always driven by the condensation of C-C_0 magnons. The C-IC magnons always lose to C-C_0 magnons before hitting the phase boundary. At the two Abelian points $\beta = 0, \pi/2$, it is in the 3D XY class. At the Abelian point $\beta = \pi/2$, C-C_0 and C-C_π magnons condense simultaneously and lead to a 3D XY class transition to the X-FM. Due to the lack of generalized mirror symmetry as in the h_x case, the C-IC regime has a more complicated landscape than that in Fig. 1. The detailed competition in the C-IC regime is shown in Figs. 6 and 12. The five dots are explained in Appendix C. As shown in [13,14], the dispersions of C-C_0, C-C_π, C-IC magnons can be mapped out by the transverse spin structure factors.

where h_z is applied along the z direction which is normal to the Rashba (α, β) SOC in the XY plane.

By applying the $U(1)_{soc}$ symmetry operator $U_1(\phi) = e^{i\phi \sum_i (-1)^x S_i^y}$ [14] to Eq. (30) and setting $\phi = \pi/2$, one can show that the $-h_z \sum_i S_i^z$ can be mapped to the RFHM in a staggered h_x field along the x direction $-h_x \sum_i (-1)^x S_i^x$. As expected, the staggered h_x could make dramatic difference than the uniform case discussed in the last section. Similar to the analysis below Eq. (2), one can see that the Hamiltonian Eq. (30) has the translational symmetry and the $\mathcal{P}_z$ symmetry. It also keeps $\mathcal{T}\mathcal{P}_x$ and $\mathcal{T}\mathcal{P}_y$ symmetry.

The main results to be achieved in this section is summarized as follows: We show that any infinitesimal h_z will change the Y-x state into a canted YZ-x state shown in Fig. 5. Unfortunately, the generalized mirror transformation used in the h_x case does not work in the h_z case anymore. This fact makes the landscapes of the C-IC magnons much more complicated in the h_z case than the h_x case. Even so, we are still able to map out the competing boundaries and detailed structures of the C-C_0, C-C_π, and C-IC magnons inside the YZ-x canted phase in Fig. 6. As h_z increases, the C-C_0 magnons still win the competition and emerge as the seeds to drive the transition from the YZ-x state to the Z-FM state at a critical field $h_{cz}(\beta)$, which is shown to be also in the universality class of 3D Ising model in Fig. 5. Due to the enlarged U(1) symmetry mentioned at the

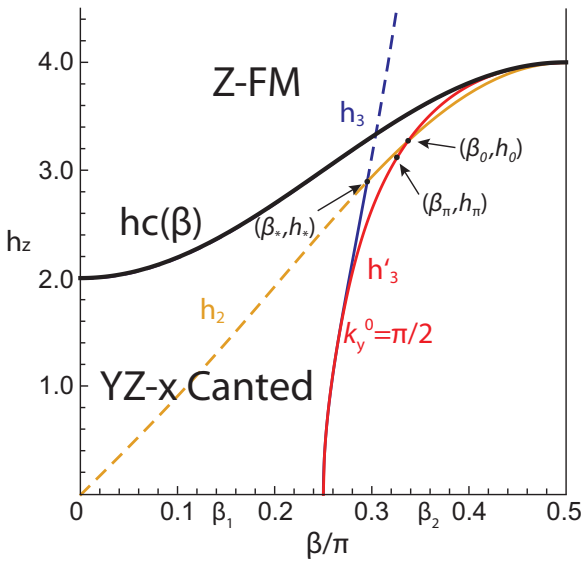

FIG. 6. Due to the lack of generalized mirror symmetry as in the h_x case in Fig. 2, one needs three separate backbone lines h_3' and h_2, h_3 to describe the competitions of the three kinds of magnons and their boundaries. The thick solid line is the phase boundary h_{cz}. The h_3' (red line) is the constant contour at $k_y^0 = \pm\pi/2$. Along the solid line parts of h_2 (brown line) and h_3 (blue line), C-C_0 and C-C_π become degenerate $\omega(k_x = 0, k_y = 0) = \omega(k_x = 0, k_y = \pi)$. The dashed parts of h_2 and h_3 are extraneous solutions. The h_3' line is split into three segments $\pi/4 < \beta < \beta_\pi$; $(0, k_0^y = \pm\pi/2)$ is the minimum position. $\beta_\pi < \beta < \beta_0$; C-$C_\pi$ becomes the minimum position. When $\beta_0 < \beta < \pi/2$, h_3' rises above h_2 and moves into the C-C_0 regime. Details are given in Appendix C.

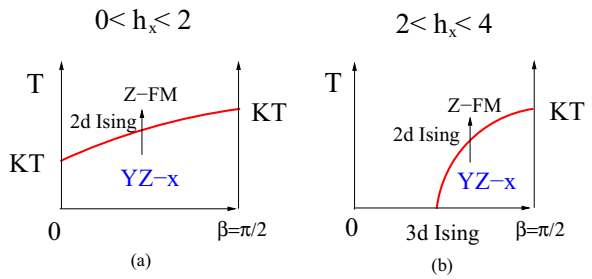

FIG. 7. Finite-temperature phase transitions (a) at a fixed $0 < h_x < 2$ and (b) at a fixed $2 < h_x < 4$.

Introduction, the transition at the two Abelian points $\beta = 0$ and $\beta = \pi/2$ point is driven by the condensation of C-C_0 and the simultaneous condensations of the C-C_0 and C-C_π magnons, respectively, and is in the universality class of the 3D XY model. In principle, all the thermodynamic quantities such as the magnetization, specific heat, uniform and staggered susceptibilities in the YZ-x canted phase, the Z-FM, and their quantum critical scalings can be calculated. We also work out the finite-temperature phase diagram in Fig. 7.

A. Z-FM state and excitations in the strong field

In a strong transverse field $H_z \gg J$, the system is in Z-FM phase with spin classically fully polarized to the S_z direction with quantum fluctuations shown in Fig. 5. Introducing the HP bosons $S^+ = \sqrt{2S - a^\dagger a}a$, $S^- = a^\dagger\sqrt{2S - a^\dagger a}$, and $S^z = S - a^\dagger a$, the Hamiltonian Eq. (30) can be written in a systematic $1/S$ expansion in terms of the HP bosons. Up to the LSW order at $1/S$, we get

$$\mathcal{H}_2 = E_0 + 2JS\sum_k[(h_z - 2\sin^2\beta - \cos^2\beta\cos k_y)a_k^\dagger a_k + (\sin^2\beta\cos k_y - \cos k_x)(a_k a_{-k} + a_k^\dagger a_{-k}^\dagger)/2], \quad (31)$$

where the classical ground-state energy $E_0 = 2JNS^2\sin^2\beta - H_zNS$ and the dimensionless field $h_z = H_z/(2JS)$. Now the Hamiltonian can be diagonalized by a Bogoliubov transformation,

$$\mathcal{H}_2 = E_0' + 4JS\sum_k \omega_k\alpha_k^\dagger\alpha_k, \quad (32)$$

where $E_0' = E_0 - 2JS\sum_k\omega_k$ is the ground-state energy at the order of $1/S$ and the spin-wave dispersion takes the form

$$\omega_k = \sqrt{(h_z - 2\sin^2\beta - \cos^2\beta\cos k_y)^2 - (\sin^2\beta\cos k_y - \cos k_x)^2}, \quad (33)$$

where, for $0 < \beta < \pi/2$, one can identify that there is a unique minimum located at $k_0 = (k_x, k_y) = (\pi, 0)$ with the gap

$$\Delta_\pi = \omega_{k=k^0} = \sqrt{h_z(h_z - 3 + \cos 2\beta)} \quad (34)$$

and the critical field strength is given by the gap vanishing condition

$$h_{cz}(\beta) = 3 - \cos 2\beta = 2 + 2\sin^2\beta, \quad (35)$$

which is shown in Fig. 5.

The excitation around the minimum $(\pi, 0)$ takes the relativistic form

$$\omega_q = \sqrt{\Delta_\pi^2 + v_x^2 q_x^2 + v_y^2 q_y^2}, \quad k = k^0 + q, \quad (36)$$

where

$$v_x^2 = 1 + \sin^2\beta, \quad v_y^2 = (h - 1)\cos^2\beta + 2\sin^4\beta, \quad (37)$$

and the critical velocities are $v_{x,c}^2 = v_{y,c}^2 = 1 + \sin^2\beta$. In contrast to the h_x case, here the $v_{x,c}$ and $v_{y,c}$ do not vanish even at $\beta = 0$. The gap vanishing at $k^0 = (k_x, k_y) = (\pi, 0)$ indicate a quantum phase transition into a spin-orbital correlated state with orbital order $(\pi, 0)$. It was known that at $h_z = 0$, the ground state Y-x state also has the $(\pi, 0)$ orbital order. That indicates that there is only one phase transition and the state below h_{cz} could be just the YZ-x state with a canted angle. As to be shown in the next section, we show that it is indeed the YZ-x state with the orbital order $(\pi, 0)$. Near the QPT, $\Delta_\pi \sim (h_z - h_{cz})^{1/2}$.

Similar to Sec. II A, before starting the next section, we discuss a little bit further the enlarged symmetry and its consequences at the two Abelian points $\beta = 0, \pi/2$ in Fig. 5.

The U(1) symmetry at the two Abelian points $\beta = 0, \pi/2$ at a finite h_z

At the two Abelian points $\beta = 0, \pi/2$ and $h_z = 0$, the system has a SU(2) symmetry in the rotated basis $\tilde{\text{SU}}(2)$ with $\tilde{\mathbf{S}}_i = R_x(i_x\pi)\mathbf{S}_i$ or $\tilde{\tilde{\text{SU}}}(2)$ with $\tilde{\tilde{\mathbf{S}}}_i = R_x(i_x\pi)R_y(i_y\pi)\mathbf{S}_i$, respectively. So Eq. (30) can be mapped to a FM Heisenberg model in $-h_z\sum_i(-1)^{i_x}\tilde{S}_i^x$ [see Eq. (38)] and $-h_x\sum_i(-1)^{i_x+i_y}\tilde{\tilde{S}}_i^x$ [see Eq. (45)], respectively. So at $\beta = 0, \pi/2$, taking the result from [18], any h_z will lead to a spin-flop transition resulting into a U(1) symmetry breaking canted phase with one Goldstone mode ϕ. Then there is another transition to the Z-FM at a finite $h_c = 2, 4$ respectively. These results at the two Abelian points fit into the general result Eq. (35) and are shown in Fig. 5.

For $(\beta = 0, h_z = 0)$, transferring back from the $\tilde{\text{SU}}(2)$ basis to the original basis, the Hamiltonian Eq. (30) has the SU(2) symmetry which is generated by $\sum_i S_i^x$, $\sum_i(-1)^{i_x}S_i^y$, and $\sum_i(-1)^{i_x}S_i^z$. When $h_z > 0$, only $\sum_i(-1)^{i_x}S_i^z$ remains as a conserved quantity. Obviously, the Z-FM state keeps all symmetry from the Hamiltonian. Having the conserved quantity $e^{i\phi\sum_i(-1)^{i_x}S_i^z}$ carrying momentum $(\pi, 0)$ act on the excitation in Eq. (36) at the minimum $(\pi, 0)$ will generate another minimum at $(0, 0)$. So we conclude that at $(\beta = 0 h_z > 0)$, the system has two minima located at $(0, 0)$ and $(\pi, 0)$, as shown in Fig. 5.

For $(\beta = \pi/2, h_z = 0)$, transferring back from the $\tilde{\tilde{\text{SU}}}(2)$ basis to the original basis, the Hamiltonian Eq. (30) has the SU(2) symmetry which is generated by $\sum_i(-1)^{i_y}S_i^x$, $\sum_i(-1)^{i_x}S_i^y$, and $\sum_i(-1)^{i_x+i_y}S_i^z$. When $h_z > 0$, only $\sum_i(-1)^{i_x+i_y}S_i^z$ remain as a conserved quantity. Having the conserved quantity $e^{i\phi\sum_i(-1)^{i_x+i_y}S_i^z}$ which carries momentum

(π,π) act on the excitation in Eq. (36) at the minimum $(\pi,0)$ generates another minimum at $(0,\pi)$. So we conclude that at $(\beta=\pi,\ h_z>0)$, the system has two minima located at $(\pi,0)$ and $(0,\pi)$, as shown in Fig. 5.

Similar to Sec. II A, the U(1) symmetry $\sum_i(-1)^{i_x}S_i^z$ or $\sum_i(-1)^{i_x+i_y}S_i^z$ at the Abelian point $\beta=0$ or $\beta=\pi/2$ at a nonzero transverse field h_z is different than the spin-orbital coupled $\mathrm{U(1)_{soc}}$ symmetry $\sum_i(-1)^{i_x}S_i^y$ along the line $(\alpha=\pi/2,\beta)$ at $h_z=0$ in the RFHM Eq. (1).

B. The coplanar *YZ-x* canted state below h_{cz}

1. *Classical YZ-x canted phase at $h<h_{cz}$*

Here we first achieve the classical YZ-x canted state from the two Abelian points.

a. Approaching to the right from the Abelian point $\beta=0$. At $\beta=0$, in the $\tilde{\mathrm{SU}}(2)$ basis $\tilde{\mathbf{S}}_i=R_x(i_x\pi)\mathbf{S}_i$, the Hamiltonian Eq. (30) takes the form

$$\mathcal{H}=-J\sum_{\langle ij\rangle}\tilde{\mathbf{S}}_i\cdot\tilde{\mathbf{S}}_j-H_z\sum_i(-1)^{i_x}\tilde{S}_i^z. \tag{38}$$

When $0<H_z<H_{zc}$ the classical state in the $\tilde{\mathrm{SU}}(2)$ basis is

$$\tilde{\mathbf{S}}_i=S(\sin\theta\cos\phi,\sin\theta\sin\phi,(-1)^{i_x}\cos\theta). \tag{39}$$

Reverting back to original basis leads to the classical state in original basis,

$$\mathbf{S}_i=S(\sin\theta\cos\phi,(-1)^{i_x}\sin\theta\sin\phi,\cos\theta), \tag{40}$$

where ϕ is nothing but the Goldstone mode due to the U(1) symmetry breaking.

Although we obtained Eqs. (39) and (40) at $\beta=0$, the same ansatz hold for $0<\beta<\pi/2$, whose classical ground energy is

$$E_c=-2NJS^2[1-(1+\sin^2\beta)\cos^2\theta+h_z\cos\theta-\sin^2\beta\sin^2\theta\cos^2\phi]. \tag{41}$$

It is easy to see that any $\beta>0$ explicitly breaks the U(1) symmetry at $\beta=0$, so picks up $\phi=\pi/2$, opens the gap [34] to the Goldstone mode ϕ and leads to the classical YZ-x canted state,

$$\mathbf{S}_i=S(0,(-1)^{i_x}\sin\theta,\cos\theta), \tag{42}$$

with the corresponding classical ground-state energy

$$E_c=-2NJS^2[1-(1+\sin^2\beta)\cos^2\theta+h_z\cos\theta]. \tag{43}$$

Minimization of Eq. (43) leads to the canted angle,

$$\cos\theta=\frac{h_z}{2(1+\sin^2\beta)}<1,\quad \text{when}\quad h_z<h_{cz}, \tag{44}$$

which always has a solution as long as $h_z<h_{cz}$.

b. Approaching to the left from the Abelian point $\beta=\pi/2$. In fact, one can reach the same results in Eqs. (42) and (43) from the right at $\beta=\pi/2$. In the $\tilde{\tilde{\mathrm{SU}}}(2)$ basis $\tilde{\tilde{\mathbf{S}}}_i=R_x(i_x\pi)R_y(i_y\pi)\mathbf{S}_i$, the Hamiltonian in Eq. (30) at $\beta=\pi/2$ takes the form

$$\mathcal{H}=-J\sum_{\langle ij\rangle}\tilde{\tilde{\mathbf{S}}}_i\cdot\tilde{\tilde{\mathbf{S}}}_j-H_z\sum_i(-1)^{i_x+i_y}\tilde{\tilde{S}}_i^z. \tag{45}$$

When $0<H_z<H_{cz}$, the classical ground state is

$$\tilde{\tilde{\mathbf{S}}}_i=S(\sin\theta\cos\phi,\sin\theta\sin\phi,(-1)^{i_x+i_y}\cos\theta). \tag{46}$$

Reverting back to the original basis leading to the classical ground state in the original basis,

$$\mathbf{S}_i=S((-1)^{i_y}\sin\theta\cos\phi,(-1)^{i_x}\sin\theta\sin\phi,\cos\theta), \tag{47}$$

with the classical ground-state energy

$$E_c=-2NJS^2[1-(1+\sin^2\beta)\cos^2\theta+h_z\cos\theta-\cos^2\beta\sin^2\theta\cos^2\phi]. \tag{48}$$

Obviously, any $\beta<\pi/2$ picks up $\phi=\pi/2$. Then Eqs. (47) and (48) reduce to Eqs. (42) and (43), respectively.

2. *Spin-wave analysis in the YZ-x canted state*

Starting from the classical YZ-x state Eq. (42) and using similar procedures to obtain Eq. (22), we obtain the spin-wave dispersion,

$$\omega_k^{\pm}=\sqrt{A_k^2+B_k^2+C_k'^2-C_k''^2-D_k^2\pm2\sqrt{(A_k^2-D_k^2)B_k^2+(A_kC_k'-C_k''D_k)^2}}, \tag{49}$$

where the expressions of A_k,B_k,D_k are listed in Eq. (20) and

$$C_k'=\sin^2\theta\cos k_x,\qquad C_k''=\cos^2\theta\cos k_x, \tag{50}$$

where one can see $C_k'+C_k''=C_k=\cos k_x$ listed in Eq. (20). Of course, the θ in Eq. (44) in the H_z field is different from that in Eq. (17) in the H_x field.

From Eq. (49), one can determine the minimum positions inside the YZ-x state. The general structure of Fig. 5 is similar to the h_x case (Fig. 1). However, due to the lack of generalized mirror symmetry as in the h_x case, the detailed landscape of the C-IC regime in Fig. 5 is much more complicated than that in the h_x case. In this section, we only outline the general structure. In the next section and Appendix C, we describe details of the shape of the C-IC regime in Fig. 5.

In Fig. 5, we still found there are three regimes inside the YZ-x canted state: C-C_0 regime, C-IC regime, and C-C_π regime which, at $h_x=0$, reduce to the three regimes identified in [14]. Among the three magnons, only C-C_0 wins the game and drives the transition, so the transition from the YZ-x state to the Z-FM is driven by the condensations of the C-C_0 magnons only. The C-IC magnons still lose to the C-C_0 in the competition.

Now we can check the consistence of the orbital orders on both sides of h_{cz}. The YZ-x state has the orbital order $(\pi,0)$; the C-C_0 has the orbital order $(0,0)=(\pi,0)$ in the RBZ. So its condensation on the top of YZ-x could lead to either of

two orbital orders, $(\pi,0)+(0,0)=(\pi,0)$ or $(\pi,0)+(\pi,0)=(0,0)$, in the EBZ. The (0,0) order is nothing but that of the Z-FM in Fig. 5.

C. Evolution of the C-IC magnons inside the C-IC regime in Fig. 5

As shown in Appendix C, the line h_3' in Fig. 6 is determined by setting the first derivative of dispersion vanishing at $(0,k_0^y=\pi/2)$. The lines h_2 and h_3 are determined by the condition that C-C_0 and C-C_π become degenerate. There is one crossing point (β_0,h_0) between h_3' and h_2 in Fig. 6.

In the h_x case discussed in Sec. II, both conditions are the same, and so lead to just one single line with the three different segments in Fig. 2 presented in Sec. II C. However, in the h_z case, there are two different conditions, which leads to three different lines h_3' and h_2,h_3, which make the detailed shape of the C-IC regime more complicated than that in h_x case.

Along the h_3', the minimum at $k_0^y=\pi/2$ stays as the (local) minima until $\beta_{\rm flat}\sim 0.33\pi$, where the second derivative of the dispersion at $(0,k_0^y=\pi/2)$ vanishes, then it becomes a maximum after $\beta>\beta_{\rm flat}$. [In fact, before getting to $\beta_{\rm flat}\sim 0.33\pi$, there is another point (let us call it β_π in Fig. 6) where the $(0,k_0^y=\pi/2)$ is just a local minimum, while the C-C_π becomes the global minimum.] Then C-C_π becomes the minimum, while C-C_0 becomes the maximum, then until C-C_π and C-C_0 becomes degenerate at $\beta_0\sim 0.337\,29\pi$ in Fig. 6. After $\beta>\beta_0$, it moves into the C-C_0 regime, where C-C_0 becomes the minimum. h_3' rises above the h_2 line. So $\beta_0\sim 0.337\,29\pi$ is determined by setting $h_2=h_3'$, as shown in Fig. 6.

So, in practice, the h_3' can be split into two segments $\pi/4<\beta<\beta_\pi$, where $(0,k_0^y=\pi/2)$ is the minimum position, and $\beta_\pi<\beta<\beta_0$, where C-C_π becomes the minimum position. (So $\beta_{\rm flat}$ is really not that important anymore.) Then when $\beta_0<\beta<\pi/2$, h_3' rises above h_2 and moves into the C-C_0 regime. Then we have to use the h_2 line to delineate the C-C_0 and C-C_π boundaries.

So the C-IC boundary along $(0,k_0^y=\pi/2)$ happens at (β_π,h_π), where it turns into C-C_π. In principle, one can determine the whole C-IC boundary in the whole YZ-x phase. Indeed, we determine the C-IC boundary along the line h_2 and h_3 in Fig. 11. Connecting all the special points along the three lines h_2,h_3,h_3' in Figs. 6 and 11 in Appendix C and also β_1,β_2 at $h_x=0$ lead to Fig. 5 and also the evolution around (β_0,h_0) in Fig. 12. As shown in [13], the I-IC dispersion can be mapped out by the transverse spin structure factors.

D. The transition from the YZ-x canted state to the Z-FM at $T=0$ and finite T

1. The $T=0$ transitions: Symmetry breaking and order parameter

The transition from the YZ-x canted state to the Z-FM at $T=0$ is still characterized by the order parameter $M_y(T=0)=\langle S^y\rangle$. As said at the beginning of Sec. III, the Hamiltonian Eq. (2) has has the translational symmetry and the $\mathcal{P}_z$ symmetry: $k_x\to -k_x$, $S^x\to -S^x$, $k_y\to -k_y$, $S^y\to -S^y$, $S^z\to S^z$. The Z-FM respects both symmetries, so $M_y(T=0)=0$, but the YZ-x states breaks both, but still keeps the combination $\mathcal{P}_z\times(x\to x+1)$, so $M_y(T=0)\neq 0$. Due to the spin-orbital locking, destroying the $M_y(T=0)=\langle S^y\rangle$ order will also restore the translational symmetry along the x direction. Similar to the h_x case, there are relativistic gapped C-C_0 magnons on both sides indicating the dynamic exponent $z=1$. So we conclude that the transition is also in the 3D Ising universality class. The LSW expansion only leads to the mean-field exponent $\beta_{MF}=1/2$, $\nu_{MF}=1/2$.

At the two Abelian points $\beta=0$ (or $\beta=\pi/2$), starting from $h>h_{cz}$, as shown in [18], due to the enlarged U(1) symmetry, the transition is driven by the simultaneous condensations of the two degenerate minima at (0,0) and $(\pi,0)$ [or $(0,\pi)$ and $(\pi,0)$] shown in Fig. 5 and is in the universality class of 3D XY model. From below $h<h_{cx}$, at $\beta=0$, it is just the condensation of C-C_0 magnons, at $\beta=\pi/2$, it is a simultaneous condensations of C-C_0 and C-C_π magnons, so the transition is also in the 3D XY universality class. After considering the above differences, the $T=0$ RG flow diagram is similar to Fig. 3.

2. The finite-temperature phase transitions

All the physical quantities at $T\ll T_{cz}$ can be similarly evaluated as in h_x case.

Because inside the YZ-x phase in Fig. 5 the RG flows to the fixed point ($\beta=\pi/4$, $h_z=0$), the finite-temperature transition at T_{cz} from the YZ-x canted phase to the Z-FM is in the same universality class as that at zero-field case shown in Fig. 3 in [14]. As argued in Sec. II D 3, it is in the 2D Ising universality class. Of course, at the two Abelian points $\beta=0,\pi/2$, it is in the 2D XY universality class. The finite-temperature transitions at the two Abelian points $\beta=0,\pi/2$ are similar to Fig. 4(a), at the mirror symmetric point $\beta=\pi/2$ is similar to Fig. 4(b). So we only show them at a given $0<h_x<4$ in Fig. 7.

IV. COMPARISONS WITH EARLIER WORKS

The C-IC magnons in the zero-field RFHM along the line $(\alpha=\pi/2,\beta)$ stand for short-ranged incommensurate orders. However, they are extrinsic, not embedded in the ground state due to the absence of quantum fluctuations in its exact ground state Y-x state. They need to be excited by thermal fluctuations or dragged out by various external probes which introduce quantum fluctuations into the ground state. In order to transfer the short-ranged incommensurate orders into long-range ordered ones, one needs to drag out these C-IC first and then drive them into condensations. However, as shown in [18] and this work, these C-IC respond quite differently to the h_y and h_x,h_z fields. In the h_y case which keeps the spin-orbital coupled $U(1)_{\rm soc}$ symmetry of the RFHM at a zero field, any small $h_y<h_{c1}$ will drag out the C-IC magnons, but the Y-x state stays as the exact ground state, so the C-IC magnons remain extrinsic, detached form the exact ground state and need to be thermally excited. As $h_y\to h_{c1}^-$, the C-IC magnons' gap collapses to the ground state and become the driving seeds to lead to various IC-SkX phase through a line of fixed points at $h_y=h_{c1}^-$. As stressed in [18] and Appendix A, from below $h<h_{c1}$, the IC-SkX is due to the condensations of nonrelativistic C-IC at a single minim $(0,k_y^0)$, so the transition at h_{c1} has the dynamic exponent $z=2$, and from above

$h > h_{c2}$, the IC-SkX is due to the simultaneous condensations of nonrelativistic C-IC at two degenerate minima at $(0,k_y^0)$ and (π,k_y^0), so the transition at h_{c2} also has the dynamic exponent $z = 2$. On the experimental side, the IC-SkX phase matches rather naturally and precisely the incommensurate, counter-rotating (in the A/B sublattice), noncoplanar magnetic orders detected on iridates α,β,γ-Li_2IrO_3 [7]. Both h_x and h_z explicitly break the spin-orbital coupled U(1) symmetry.

However, any small h_x and h_z will transfer Y-x state into the YX-x or YZ-x phase, respectively, which support only gapped magnons. Unfortunately, as shown in Figs. 1 and 5, as h_x and h_z increase, the relativistic C-IC with at least two minima at $(0,\pm k_y^0)$ always lose to C-C_0, so cannot emerge to drive any phase transitions. There is only one transition to the X-FM or Z-FM which is driven by the condensation of C-C_0 and is in the 3D Ising universality class with the dynamic exponent $z = 1$. So there is no chance to get any incommensurate phases.

In the (β,h_y) phase diagram, the IC-SkX phase is surrounded by four other phases: the two commensurate coplanar canted phases at the left and right in the SOC parameters and two collinear phases Y-x and Y-FM in the low and high field, respectively. The two canted phases and the IC-SkX phases break the U(1) symmetry spontaneously, so support a gapless excitation. The two canted phases in the h_y case are *dramatically different* than the YX-x and YZ-x canted phases in the h_x and h_y cases. The former breaks the U(1) symmetry spontaneously, does not support any C-IC magnons, but supports the gapless Goldstone mode at the $(\pi,0)$. There is no direct transition from the Y-x state to the canted state, there is always an IC-SkX phase sandwiched between the two. There is a direct transition from the canted phase to the Y-FM phase through a roton condensation at (0,0) and to the IC-SkX phase through a bosonic Lifshitz transition.

However, both h_x and h_z explicitly break the spin-orbital coupled U(1) symmetry. Any small h_x and h_z will transfer the Y-x state into the YX-x or YZ-x canted phases, respectively, which are essentially the same phase as the Y-x phase. So naturally, they also support gapped C-C_0, C-C_π, and C-IC magnons. In fact, one can also group h_y and h_x as an in-plane field and h_z in Eq. (30) as the perpendicular field. In the in-plane case, there is a mirror symmetry or a generalized mirror symmetry, respectively, to characterize the competition among the magnons, while in the perpendicular field there is no such mirror symmetry. Of course, the finite-temperature transitions in h_y and h_x,h_z cases shown in Figs. 4 and 7 are also quite different.

In a recent preprint [13], we studied the rotated antiferromagnetic Heisenberg model (RAFHM), which is the fermionic analog of the RFHM [14]. We found that the C-C_0 and C-IC magnons in the RAFHM are also intrinsic ones generated by quantum fluctuations, take relativistic dispersion, and are already embedded in the ground state. Their parameters such as the minimum positions $(0,\pm k_y^0)$, gap, and velocities v_x,v_y can be precisely measured by the peak positions, width, and Lorentzian shape of the transverse structure factor at $T = 0$, respectively. In this sense, the relativistic C-C_0 and C-IC magnons in the Y-y state in the RAFHM at zero field resemble those in the YX-x and YZ-x canted states studied in this paper.

In this work, we only focus along $(\alpha = \pi/2,\beta)$ in a transverse field h_x or h_z. Obviously, it is important to study how these magnons respond when $\alpha \neq \pi/2$ (but at zero field), which also explicitly breaks the spin-orbital coupled U(1) symmetry at $\alpha = \pi/2$. This investigation is complementary to $(\alpha = \pi/2,\beta)$ in a nonzero field h_x or h_z studied in this paper. It has been achieved in a very recent preprint [35], where we showed that turning on $\alpha \neq \pi/2$ leads to new competitions very different from the two Zeeman field cases studied here, which, in turn, leads to different phases and phase transitions.

V. DISCUSSIONS AND CONCLUSIONS

It is easy to see why the transition from YX-x to X-FM in Fig. 1 and YZ-x to Z-FM in Fig. 5 have to go through C-C_0 instead of C-C_π. This is because YX-x or YZ-x have the orbital order $(\pi,0)$ and the C-C_0 has the orbital order $(0,0) = (\pi,0)$ in the RBZ. So its condensation on the top of YX-x or YZ-x order could lead to two orbital orders, either $(\pi,0) + (0,0) = (\pi,0)$ or $(\pi,0) + (\pi,0) = (0,0)$ in the EBZ. The (0,0) order is nothing but that of the X-FM in Fig. 1 or Z-FM in Fig. 5. However, the C-C_π has the orbital order $(0,\pi) = (\pi,\pi)$ in the RBZ. So its condensation on the top of YX-x or YZ-x order could lead to two orbital orders, either $(\pi,0) + (0,\pi) = (\pi,\pi)$ or $(\pi,0) + (\pi,\pi) = (0,\pi)$, in the EBZ; none of the two contains the (0,0) order. So C-C_π alone cannot drive the transition to X-FM or Z-FM.

We established our results at the LSW order. Following [13], one can perform the $1/S$ corrections due to the magnon interactions to the results at the LSW order. We expect that the correction is very tiny even at $s = 1/2$, as found in [13], except very close to the quantum phase transitions in Fig. 1 and 5. So we expect that the competition boundaries among different magnons in Figs. 2 and 6 suffer very little shift. As shown in [13], the dispersions of the magnons, and therefore their boundaries in Figs. 2 and 6, can be mapped out by structure factors which can be detected by Bragg spectroscopy [32,33] in the cold-atom experiments or magnetic inelastic x-ray scattering in materials with strong SOC [22–24]. Of course, different spin-orbital correlated magnetic orderings in Figs. 1 and 5 and the finite-temperature phase transitions between them in Figs. 4 and 7 can be detected by similar experimental techniques.

It is instructive to compare the C-IC magnons with quantum fluctuations generated in multiple vortices in p/q filling Boson Hubbard models [36–39], those in high-T_c superconductors [40,41], and exciton superfluids in Bilayer or trilayer quantum Hall systems [8,9]. The vortices are gapped topological excitations inside a superfluid; there are at least q degenerate minima in their dispersions which transform to each other under the projective representation of the magnetic space group (MSG). So the gap closing (or condensations) of the q minima lead to various kinds of lattice symmetry-breaking insulating states. So these quantum fluctuations generated vortices are short-range translational symmetry-breaking insulating orders embedded inside the translational invariant superfluid states. Even inside the superfluid state, they are the crucial ingredients of the superfluid ground state and are generated by the intrinsic quantum fluctuations. Their condensations tuned by interactions spark quantum phase transitions into various neighboring insulating states, breaking various translational symmetries of lattices. Of course, vortices

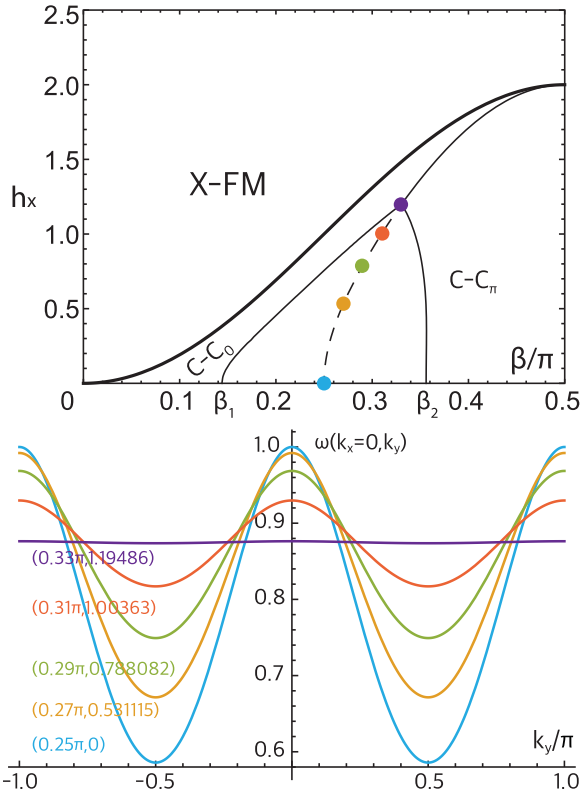

FIG. 8. (Top) Phase diagram in the h_x case. The dashed line indicates the contour $k_y^0 = \pm\pi/2$ inside the C-IC regime. Colored dots stand for the five parameters $[\beta, h(\beta)]$—$(0.25\pi, 0)$, $(0.27\pi, 0.531\,115)$, $(0.29\pi, 0.788\,082)$, $(0.31\pi, 1.003\,63)$, $(0.33\pi, 1.194\,86)$—used for the figure falling in the range $\pi/2 < \beta < \beta_0 \approx 0.330\,458\pi$. (Bottom) Spin-wave spectrum corresponding to the four dots in the top figure. There are no other contours crossing the $k_y^0 = \pi/2$ contour in this range. For example, the contour $k_y^0 = \pi/2 + 10^{-5}$ will hit the extension of the contour $k_y^0 = \pi/2$ in the range $\beta_0 \leqslant \beta \leqslant \beta_*$ (see Fig. 9). As h_x increases, the gap at $k_y^0 = \pm\pi/2$ increases. Note that even at $\beta = 0.33\pi$, $h = 1.194\,86$ the spectrum is dispersive instead of being a flat line.

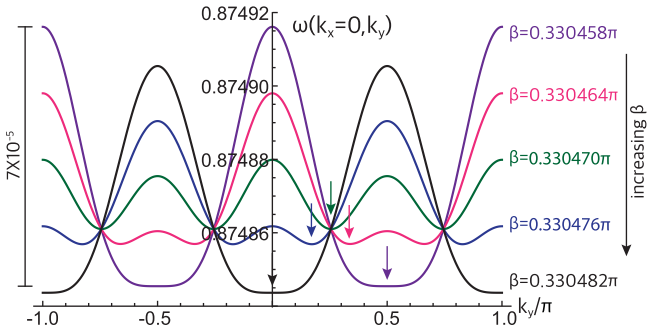

FIG. 9. The spin-wave spectrum for several $[\beta, h(\beta)]$ in the range $\beta_0 \leqslant \beta \leqslant \beta_*$ in the top part of Fig. 8. The arrow are guides to the minima locations. Due to the generalized mirror symmetry, there are four degenerate minima which are symmetric with respect to $k_y = \pm\pi/2$, respectively. Due to the $k_y \to -k_y$ symmetry, the four minima are also symmetric with respect to $k_y = 0$. As increasing β from β_0 to β_*, the minima positions continuously shift from $\pi/2$ to either 0 or π. For the red curve ($\beta = 0.330\,464\pi$), the four degenerate minima are at $k_y^0 = \pm\pi/3, \pm 2\pi/3$. It also indicates that the fpour contours will hit the extension of the contour $k_y^0 = \pm\pi/2$ at $\beta = 0.330\,464\pi$ shown in Fig. 2.

are bosons and satisfy boson statistics. Here these C-C$_0$, C-C$_\pi$, and C-IC gapped magnons inside the YX-x or YZ-x state play similar roles as the vortices inside a translational invariant superfluid state. They are the crucial ingredients of the YX-x or YZ-x state and are generated by the intrinsic quantum fluctuations. Their condensations tuned by various Zeeman fields spark quantum phase transitions into various neighboring spin-orbital correlated commensurate or incommensurate phases. The salient feature of the C-IC magnons is that they may condense at any incommensurate wave vector leading to incommensurate spin-orbital correlated magnetic phases. This is indeed what happens in the h_y Zeeman field studied in [18]. However, in the h_x, h_z fields studied in this paper, they are eliminated before their possible condensations.

The multiple local (metastable) or global minima structure of the C-IC magnons shown in Figs. 8, 9, and 10 indicate some short-ranged quantum fluctuations with multiple length scales. The complex structure is intrinsic and embedded in the quantum ground state, which may resemble the complex multiple local minimum landscapes in quantum spin glass [42–45]. However, the former is SOC induced; the latter is due to quenched disorders. So the SOC may induce some similar complex phenomena as the disorders do.

One of the original goals of studying the SOC effects in quantum spin systems is to look for possible spin-liquid phases. It is generally assumed [46] that in the presence of SOC, the spin rotation symmetry is completely broken, so the Lieb-Schultz-Mattis-Oshikawa-Hastings (LSMOH) theorem [47–49] may not apply. However, Oshikawa's arguments [48] require only U(1) symmetry with the S^z conservation instead of the full SU(2) symmetry. The quantum spin Hall effect in the Kane-Mele model [50] in a honeycomb lattice is an Abelian SOC case with the S^z conservation. Of course, in the Kane-Mele model, the additional possible Rashba or Dresselhaus SOC spoils the U(1) symmetry, but the time-reversal symmetry $\mathcal{T}$ remains. The line $(\alpha = \pi/2, \beta)$ at zero field is the first non-Abelian SOC case which still owns a spin-orbital coupled U(1) symmetry. At filling factor $n = 1$, there is also only one spin $s = 1/2$ per unit cell in the original basis. In the U(1) basis [14], it becomes an explicit U(1) symmetry with the expense of breaking the translational symmetry of the Hamiltonian to two sites per unit cell. So when trying to apply the Oshikawa's argument in the U(1) basis, one run into two spin-1/2's per unit cell, so it still does not apply. Then the possible new mechanisms [46] only assuming $\mathcal{T}$ may apply to search for possible spin-liquid states in the presence of SOC in some lattices. The longitudinal [18] Zeeman field h_y still keeps the U(1) symmetry, but breaks the $\mathcal{T}$ symmetry. Here the two transverse fields break both the U(1)$_{\rm soc}$ symmetry and the time reversal explicitly, so it is not surprising that we only find the symmetry-breaking ground states shown in Figs. 1 and 5 instead of any spin-liquid ground state in a square lattice. Note that in a previous study of a frustrated Ising model in a transverse field [25,26], due to its violation of both the LSMOH condition and the time-reversal symmetry, no spin liquids were found either.

In this work, we focus only on quantum phases with only bosonic excitations and without topological orders. It can be considered as incorporating possible dramatic effects of SOC on a well-studied 2D Ising, anisotropic (or isotropic) quantum XY model in a transverse field [5]. As said in the Introduction, in fermionic systems [8–13], the quantum phase supports both fermionic excitation and collective bosonic excitations. The two sectors may compete to lead to various other quantum phases under various external probes. In a recent preprint [51], we studied the attractive Hubbard model with Rashba or Dresselhaus spin-orbit coupling in a 2D square lattice subject to a perpendicular h_z field which is the weak-coupling and negative-interaction cousin of Eq. (30). We find it is the touching (or gap closing) of fermionic quasiparticle excitations which signifies a topological transition from a topological SF to a trivial one or to a band insulator. Obviously, a fermionic quasiparticle cannot condense, but they could change the topological winding numbers and therefore spark topological transitions. It remains much more challenging to study topological confinement and deconfinement transitions driven by condensations of fractionized particles satisfying Abelian or non-Abelian statistics [4,6]. Unfortunately, in contrast to bosonic or fermionic excitations which are only short-range entangled, one may not be able to treat these fractionized particles as independent particles due to the long-range entanglements meditated by Abelian or non-Abelian Chern-Simon interactions [4,6,40,52,53].

ACKNOWLEDGMENTS

We acknowledge Grants No. NSF-DMR-1161497 and No. NSFC-11174210 for supports. The work at KITP was supported by Grant No. NSF PHY11-25915. W.M.L. is supported by NSFC under Grants No. 11434015, No. 61227902, and No. 61378017, NKBRSFC under Grants No. 2012CB821305, SKLQOQOD under Grants No. KF201403, and SPRPCAS under Grants No. XDB01020300.

APPENDIX A: ENERGY SPECTRUM SYMMETRY ANALYSIS OF THE YX-x STATE IN THE h_x CASE AND THE YZ-x STATE IN THE h_z CASE

The zero-field RFHM studied in [14] has the translational symmetry and the $\mathcal{T}$, $\mathcal{P}_x$, $\mathcal{P}_y$, and $\mathcal{P}_z$ symmetry. Along the line $(\alpha = \pi/2, \beta)$, it also has the spin-orbital coupled U(1) symmetry $[H, \sum_i (-1)^{i_x} S_i^y] = 0$. Under the local rotation $\vec{\tilde{S}}_i = R_x(\pi) R_y(i_y \pi) \vec{S}_i$ and $\beta \to \pi/2 - \beta$. At the middle point $\beta = \pi/4$, the Hamiltonian is invariant under such a transformation. The Y-x state breaks all these symmetries except the U(1) symmetry and the $\mathcal{P}_y$ symmetry: $S^y \to S^y$, $k_x \to -k_x$, $S^x \to -S^x$, $S^z \to -S^z$. However, it still keeps $\mathcal{P}_x \times (x \to x+1)$ and $\mathcal{P}_z \times (x \to x+1)$ symmetry, so the excitation spectrum must have the $k_y \to -k_y$ symmetry also, as indeed respected by the LSW spectrum shown in [14]. At $\beta = \pi/4$, the Y-x state also keeps the $\vec{\tilde{S}}_i = R_x(\pi) R_y(i_y \pi) \vec{S}_i$ followed by the $\mathcal{T}$, which is called the mirror symmetry $\mathcal{M}$ in [18].

The RFHM in the longitudinal h_y field enjoys the translational symmetry and the $\mathcal{P}_y$ symmetry, breaks $\mathcal{P}_x$,$\mathcal{P}_y$, of course, breaks $\mathcal{P}_x \times (x \to x+1)$ and $\mathcal{P}_z \times (x \to x+1)$ symmetry, but still keeps $\mathcal{T}\mathcal{P}_x$ and $\mathcal{T}\mathcal{P}_y$. Along the line $(\alpha = \pi/2, \beta)$, it keeps the spin-orbital coupled U(1) symmetry. At $\beta = \pi/4$, it also keeps the $\mathcal{M}$ symmetry: The Y-x state at $h < h_{c1}$ keeps $\mathcal{P}_y$ symmetry, but breaks the translational symmetry by one lattice site $(x \to x+1)$, so the excitation spectrum may not have the $k_y \to -k_y$ symmetry anymore. Indeed, the h_y field just picks one of the two degenerate minima $\pm k_y^0$ and condenses it at $h = h_{c1}$, as shown in Fig. 1 in [18].

As said at the beginning of Sec. II, the RFHM in the h_x transverse field Eq. (2) enjoys the $\mathcal{P}_x$ symmetry—$S^x \to S^x$, $k_y \to -k_y$, $S^y \to -S^y$, $S^z \to -S^z$—and the translational symmetry. The YX-x state breaks both the $\mathcal{P}_x$ symmetry and the translational symmetry by one lattice site $(x \to x+1)$, but keeps the combination of the two $\mathcal{P}_x \times (x \to x+1)$. So the excitation spectrum must have the $k_y \to -k_y$ symmetry. This is indeed respected by the LSW spectrum shown in Figs. 2, 8, and 9.

Very similarly, as said at the beginning of Sec. III, the RFHM in the h_z transverse field Eq. (30) enjoys the translational symmetry and the $\mathcal{P}_z$ symmetry—$k_x \to -k_x$, $S^x \to -S^x$, $k_y \to -k_y$, $S^y \to -S^y$, $S^z \to S^z$—which is also equivalent to a joint π rotation of both the spin and the orbital around the $\hat{z}$ axis. The YZ-x state breaks both the $\mathcal{P}_z$ symmetry and the translational symmetry by one lattice site $(x \to x+1)$, but keeps the combination of the two $\mathcal{P}_z \times (x \to x+1)$. So the excitation spectrum must have the $k_y \to -k_y$ symmetry also. This is indeed respected by the LSW spectrum shown in Figs. 10 and 11.

Both h_x and h_z break the U(1) symmetry. There is also no mirror transformation anymore. This leads to dramatic different responses of the magnons under h_x,h_z studied in this paper than those in the h_y investigated in [18].

APPENDIX B: THE EVOLUTION OF C-IC IN h_x CASE

As motivated in Sec. II C, we like to investigate possible "generalized" mirror symmetry around $k_y = \pi/2$. So we apply

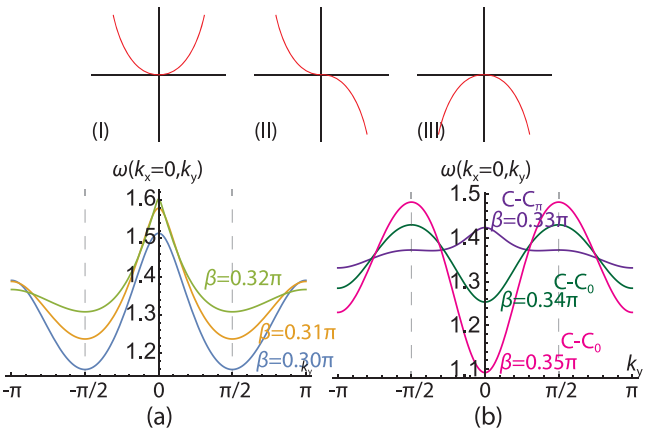

FIG. 10. (Top) When β increases from $\pi/4$ to $\pi/2$ along h_3', the contour extreme at $k_y^0 = \pm\pi/2$ goes through (I) concave, (II) inflection point, and (III) convex (namely $\frac{\partial^2 \omega_k}{\partial k_y^2}|_{k=(0,\pi/2)} > 0, = 0, < 0$), with the inflection point sitting at $\beta_{flat} \approx (0.328 \pm 0.001)\pi$. (Bottom) The spin-wave dispersion along h_3' for different β: (a) $0.30\pi, 0.31\pi, 0.32\pi$ falling in the range $\pi/4 < \beta < \beta_{\text{flat}}$, $k_y^0 = \pm\pi/2$ is at least a local minimum; (b) 0.33π, 0.34π, 0.35π falling in the range $\beta_{\text{flat}} < \beta < \pi/2$. $k_y^0 = \pm\pi/2$ becomes at least a local maximum.

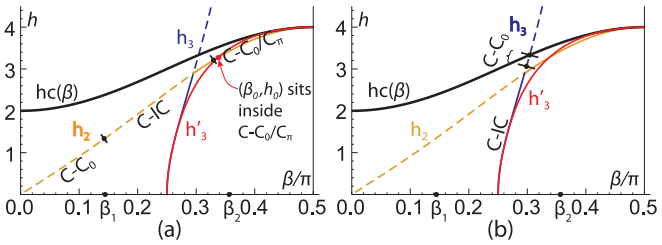

FIG. 11. (a) Along h_2, the minimum location of the dispersion is $k = (0,0)$, then becomes $k = (0,0 < k_y^0 < \pi)$, and then becomes either $k = (0,0)$ or $k = (0,\pi)$, which are degenerate along h_2. (b) Along h_3, the minimum location of the dispersion is $k = (0,0 < k_y^0 < \pi)$ and then becomes $k = (0,0)$.

a shift $k = (0,\pi/2) + q$ to the dispersion Eqs. (22) and (20) and get

$$\begin{aligned} A_q &= 2 + (\cos^2\beta - \sin^2\beta\sin^2\theta)\sin q_y, \\ B_q &= \sin 2\beta \sin\theta \cos q_y, \\ C_q &= \cos q_x, \\ D_q &= -\sin^2\beta\cos^2\theta\sin q_y. \end{aligned} \tag{B1}$$

It is easy to see that the only term which is not mirror symmetric with respect to $q_y = 0$ is contained in A_q. [D_q has no problem because it is squared in Eq. (22).] Making the spectrum mirror symmetric with respect to $q_y = 0$ dictates

$$\cos^2\beta - \sin^2\beta\sin^2\theta = 0. \tag{B2}$$

Plugging in the Eq. (17) leads to Eqs. (25) and (26).

Equation (26) is obtained demanding that the energy spectrum is symmetric with respect to $k_y^0 = \pi/2$, so it guarantees it must be an extreme (either minimum or maximum) at $k_y^0 = \pi/2$ and also the degeneracy condition $\omega_{k=(0,0)} = \omega_{k=(0,\pi)}$. This explains why Eq. (26) also contains the C-C$_0$/C-C$_\pi$ boundary Eq. (25).

APPENDIX C: THE EVOLUTION OF *C-IC* IN h_z CASE

Following the procedures in the h_x case, we first determine the boundary between C-C$_0$ and C-C$_\pi$ by setting $\omega_k^-(0,0) = \omega_k^-(0,\pi)$. Using Eq. (49), we find it has four positive roots h_1,h_2,h_3,h_4 and four negative roots. After comparing with numerical results, we find only the two roots, h_2 and h_3, are physical:

$$\begin{aligned} h_2 &= \sqrt{2(3-\cos 2\beta)(1-\cos 2\beta)}, \\ h_3 &= (3-\cos 2\beta)\sqrt{\frac{-2\cos 2\beta}{1+\cos 2\beta}}. \end{aligned} \tag{C1}$$

Setting $h_2 = h_3$ leads to $\beta = \beta_* = 0.295\,296\pi$, as shown in Fig. 6. When $0.25\pi < \beta < \beta_*$, $h = h_3$, when $\beta_* < \beta < \pi/2$, $h = h_2$.

Next we determine the constant contour at $k_y^0 = \pi/2$; thus, we need solve $0 = \frac{\partial\omega_k^-}{\partial k_y}|_{k=(0,\pi/2)}$, which leads to a quartic equation in h^2,

$$c_8h^8 + c_6h^6 + c_4h^4 + c_2h^2 + c_0 = 0, \tag{C2}$$

where the coefficients c_8,c_6,c_4,c_2,c_0 are functions of β. This equation also has four positive roots h_1',h_2',h_3',h_4' and four negative roots; we find that only h_3' is a physical solution. Its analytic expression is complicated, so we only show its numerical solution in Fig. 6. Setting $h_2 = h_3'$ leads to $\beta = \beta_0 = 0.333\,729\pi$; the three lines h_2,h_3,h_3' and their crossings are drawn in Fig. 6.

Since we set $0 = \frac{\partial\omega_k}{\partial k_y}|_{k=(0,\pi/2)}$, the dispersion around $k_y = \pm\pi/2$ changes, as shown in Fig. 10.

We can summarize the evolution along the h_3' line in the following.

Along h_3', when $0.25\pi < \beta < \beta_{\rm flat}$, $(0,\pi/2)$ is a local minimum; when $\beta_{\rm flat} < \beta < \pi/2$, $(0,\pi/2)$ is a local maximum.

Along h_3', when $0.25\pi < \beta < \beta_{t2}$, $(0,0)$ is a local maximum; when $\beta_{t2} < \beta < \pi/2$, $(0,0)$ is a local minimum.

Along h_3', when $0.25\pi < \beta < \beta_{t1}$, $(0,\pi)$ is a local maximum; when $\beta_{t1} < \beta < \pi/2$, $(0,\pi)$ is a local minimum.

The relation between these β are $\beta_{t1} < \beta_{\rm flat} < \beta_{t2}$.

If $0.25\pi < \beta < \beta_{t1}$, $(0,\pi/2)$ is a global minimum.

If $\beta_{t1} < \beta < \beta_{\rm flat}$, we need compare $(0,\pi/2)$ with $(0,\pi)$;
  if $\beta_{t1} < \beta < \beta_{tf}$, $(0,\pi/2)$ is a global minimum;
  if $\beta_{tf} < \beta < \beta_{\rm flat}$, $(0,\pi)$ is a global minimum.

If $\beta_{\rm flat} < \beta < \beta_{t2}$, $(0,\pi)$ is a global minimum.

If $\beta_{t2} < \beta < \pi/2$, we need compare $(0,\pi)$ with $(0,0)$;
  if $\beta_{t2} < \beta < \beta_0$, $(0,\pi)$ is a global minimum;
  if $\beta_0 < \beta < \pi/2$, $(0,0)$ is a global minimum.

As summarized in Sec. III C, if $0.25\pi < \beta < \beta_{tf}$, $(0,\pi/2)$ is a global minimum; if $\beta_{tf} < \beta < \beta_0$, $(0,\pi)$ is a global minimum; if $\beta_0 < \beta < \pi/2$, $(0,0)$ is a global minimum. The final result is shown in Fig. 6

The minimum structure along h_2 and h_3 are shown in Fig. 11(a) and 11(b), respectively.

Combining all the special points along the three lines h_2,h_3,h_3' in Figs. 6 and 11 and also β_1,β_2 at $h_x = 0$ leads to Fig. 5 and the evolution around (β_0,h_0) in Fig. 12.

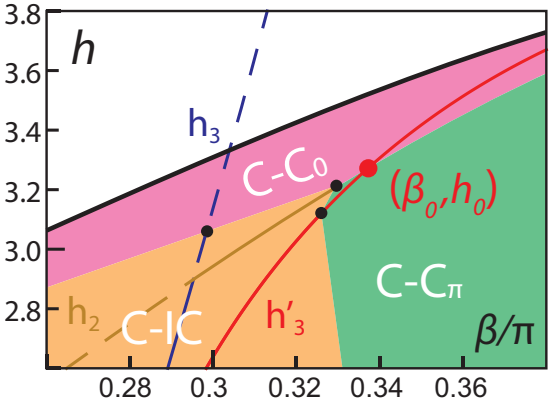

FIG. 12. Fine structure of C-C$_0$, C-IC, and C-C$_\pi$ boundaries around (β_0,h_0). It is reached by connecting those special points along the three lines h_2 (solid and dashed brown), h_3 (solid and dashed blue), and h_3' (solid red) in Figs. 6 and 11. The thick solid black line is the phase boundary h_{cz}.

[1] S. Sachdev and J. Ye, Universal Quantum-Critical Dynamics of Two-Dimensional Antiferromagnets, Phys. Rev. Lett. **69**, 2411 (1992).

[2] A. V. Chubukov, S. Sachdev, and J. Ye, Theory of two-dimensional quantum Heisenberg antiferromagnets with a nearly critical ground state, Phys. Rev. B **49**, 11919 (1994).

[3] A. Auerbach, *Interacting Electrons and Quantum Magnetism* (Springer Science & Business Media, New York, 1994).

[4] X. G. Wen, *Quantum Field Theory of Many-body Systems, From the Origin of Sound to an Origin of Light and Electrons* (Oxford University Press, Oxford, U.K., 2004).

[5] S. Sachdev, *Quantum Phase Transitions*, 2nd ed. (Cambridge University Press, Cambridge, U.K., 2011).

[6] E. Fradkin, *Field Theory of Condensed Matter*, 2nd ed. (Cambridge University Press, Cambridge, U.K., 2013).

[7] A. M. Turner and A. Vishwanath, Beyond band insulators: Topology of semi-metals and interacting phases, arXiv:1301.0330.

[8] Longhua Jiang and Jinwu Ye, Ground state, quasihole and a pair of quasihole wavefunctions in Bi-layer Quantum Hall systems, Phys. Rev. B **74**, 245311 (2006).

[9] Jinwu Ye, Broken symmetry, excitons, gapless modes, and topological excitations in trilayer quantum Hall systems, Phys. Rev. B **71**, 125314 (2005).

[10] F. Sun, X.-L. Yu, J. Ye, H. Fan, and W.-M. Liu, Topological quantum phase transition in synthetic non-Abelian gauge potential: Gauge invariance and experimental detections, Sci. Rep. **3**, 2119 (2013).

[11] Shang-Shun Zhang, Jinwu Ye, and Wu-Ming Liu, Itinerant magnetic phases and Bosonic Lifshitz transitions in repulsively interacting spin-orbit coupled Fermi gas, arXiv:1403.7031.

[12] Yi-Xiang Yu, Jinwu Ye, and Wu-Ming Liu, Cherence length in attractively interacting Fermi gases with spin-orbit couplings, Phys. Rev. A **90**, 053603 (2014).

[13] Fadi Sun, Jinwu Ye, and Wu-Ming Liu, Hubbard model with Rashba or Dresselhaus spin-orbit coupling and rotated antiferromagnetic Heisenberg model, arXiv:1601.01642.

[14] Fadi Sun, Jinwu Ye, and Wu-Ming Liu, Quantum magnetism of spinor bosons in optical lattices with synthetic non-Abelian gauge fields, Phys. Rev. A **92**, 043609 (2015).

[15] Zi Cai, Xiangfa Zhou, and Congjun Wu, Magnetic phases of bosons with synthetic spin-orbit coupling in optical lattices, Phys. Rev. A **85**, 061605(R) (2012); for a review, see, Xiangfa Zhou, Yi Li, Zi Cai, and Congjun Wu, Unconventional states of bosons with the synthetic spin Corbit coupling, J. Phys. B: At. Mol. Opt. Phys. **46**, 134001 (2013).

[16] J. Radic, A. Di Ciolo, K. Sun, and V. Galitski, Exotic Quantum Spin Models in Spin-Orbit-Coupled Mott Insulators, Phys. Rev. Lett. **109**, 085303 (2012).

[17] William S. Cole, Shizhong Zhang, Arun Paramekanti, and Nandini Trivedi, Bose-Hubbard Models with Synthetic Spin-Orbit Coupling: Mott Insulators, Spin Textures, and Superfluidity, Phys. Rev. Lett. **109**, 085302 (2012).

[18] Fadi Sun, Jinwu Ye, and Wu-Ming Liu, Rotated Heisenberg model in a Zeeman field and its applications to cold atoms and materials with spin-orbit coupling, arXiv:1502.05338.

[19] A. Kitaev, Anyons in an exactly solved model and beyond, Ann. Phys. **321**, 2 (2006). In the context of the present paper, the difference between honeycomb and a square lattice is not essential.

[20] I. Dzyaloshinskii, A thermodynamic theory of weak ferromagnetism of antiferromagnetics, J. Phys. Chem. Solids **4**, 241 (1958).

[21] T. Moriya, Anisotropic superexchange interaction and weak ferromagnetism, Phys. Rev. **120**, 91 (1960).

[22] A. Biffin, R. D. Johnson, I. Kimchi, R. Morris, A. Bombardi, J. G. Analytis, A. Vishwanath, and R. Coldea, Noncoplanar and Counterrotating Incommensurate Magnetic Order Stabilized by Kitaev Interactions in γ-Li_2IrO_3, Phys. Rev. Lett. **113**, 197201 (2014).

[23] A. Biffin, R. D. Johnson, S. Choi, F. Freund, S. Manni, A. Bombardi, P. Manuel, P. Gegenwart, and R. Coldea, Unconventional magnetic order on the hyperhoneycomb Kitaev lattice in β-Li_2IrO_3: Full solution via magnetic resonant x-ray diffraction, Phys. Rev. B **90**, 205116 (2014).

[24] Itamar Kimchi, Radu Coldea, and Ashvin Vishwanath, Unified theory of spiral magnetism in the harmonic-honeycomb iridates α,β, and γLi_2IrO_3, Phys. Rev. B **91**, 245134 (2015).

[25] R. Moessner, S. L. Sondhi, and P. Chandra, Two-Dimensional Periodic Frustrated Ising Models in a Transverse Field, Phys. Rev. Lett. **84**, 4457 (2000).

[26] R. Moessner and S. L. Sondhi, Ising models of quantum frustration, Phys. Rev. B **63**, 224401 (2001).

[27] Lianghui Huang *et al.*, Experimental realization of a two-dimensional synthetic spin-orbit coupling in ultracold Fermi gases, Nat. Phys. **12**, 540 (2016).

[28] Zhan Wu *et al.*, Realization of two-dimensional spin-orbit coupling for Bose-Einstein condensates, arXiv:1511.08170.

[29] J. Kinast *et al.*, Heat capacity of a strongly interacting Fermi gas, Science **307**, 1296 (2005).

[30] M. J. H. Ku *et al.*, Revealing the superfluid lambda transition in the universal thermodynamics of a unitary Fermi gas, Science **335**, 563 (2012).

[31] N. Gemelke, X. Zhang, C. L. Huang, and C. Chin, *In situ* observation of incompressible Mott-insulating domains in ultracold atomic gases, Nature (London) **460**, 995 (2009).

[32] J. Ye, J. M. Zhang, W. M. Liu, K. Zhang, Y. Li, and W. Zhang, Light-scattering detection of quantum phases of ultracold atoms in optical lattices, Phys. Rev. A **83**, 051604(R) (2011).

[33] J. Ye, K. Y. Zhang, Y. Li, Y. Chen, and W. P. Zhang, Optical Bragg, atom Bragg and cavity QED detections of quantum phases and excitation spectra of ultracold atoms in bipartite and frustrated optical lattices, Ann. Phys. **328**, 103 (2013).

[34] In sharp contrast, the Goldstone mode ϕ remains in the canted phase in the longitudinal case in Ref. [18].

[35] Fadi Sun, Jinwu Ye, and Wu-Ming Liu, Global quantum phase diagram of strongly interacting spinor bosons with generic 2 dimensional spin-orbital couplings in a square lattice, arXiv:1603.00451.

[36] L. Jiang and J. Ye, The mobility of dual vortices in honeycomb, square, triangular, kagome and dice lattices, J. Phys. Condens. Matter **18**, 6907 (2006).

[37] J. Ye, Duality, Magnetic space group and their applications to quantum phases and phase transitions on bipartite lattices in several experimental systems, Nucl. Phys. B **805**, 418 (2008).

[38] Y. Chen and J. Ye, Characterizing boson orders in lattices by vortex degree of freedoms, Philos. Mag. **92**, 4484 (2012).

[39] J. Ye and Y. Chen, Quantum phases, Supersolids and quantum phase transitions of interacting bosons in frustrated lattices, Nucl. Phys. B **869**, 242 (2013).
[40] Jinwu Ye, Quantum fluctuation generated vortices, dual singular-gauge transformation, and zero-temperature transition from d-wave superconductor to underdoped regime, Phys. Rev. B **65**, 214505 (2002).
[41] Jinwu Ye, Thermally Generated Vortices, Gauge Invariance, and Electron Spectral Function in the Pseudogap Regime, Phys. Rev. Lett. **87**, 227003 (2001).
[42] J. Ye, S. Sachdev, and N. Read, A Solvable Spin Glass of Quantum Rotors, Phys. Rev. Lett. **70**, 4011 (1993).
[43] S. Sachdev and J. Ye, Gapless Spin-Fluid Ground State in a Random Quantum Heisenberg Magnet, Phys. Rev. Lett. **70**, 3339 (1993).
[44] N. Read, S. Sachdev, and J. Ye, Landau theory of quantum spin glasses of rotors and Ising spins, Phys. Rev. B **52**, 384 (1995).
[45] M. P. Kennett, C. Chamon, and Jinwu Ye, Aging dynamics of quantum spin-glass of rotors, Phys. Rev. B **64**, 224408 (2001).
[46] Haruki Watanabe *et al.*, Proc. Natl. Acad. Sci. U.S.A. **112**, 14551 (2015).
[47] E. Lieb, T. Schultz, and D. Mattis, Ann. Phys. **16**, 407 (1961).
[48] M. Oshikawa, Phys. Rev. Lett. **84**, 1535 (2000).
[49] M. B. Hastings, Phys. Rev. B **69**, 104431 (2004).
[50] C. L. Kane and E. J. Mele, Quantum Spin Hall Effect in Graphene, Phys. Rev. Lett. **95**, 226801 (2005).
[51] Yi-Xiang Yu, Fadi Sun, Jinwu Ye, and Ningfang Song (unpublished).
[52] Jinwu Ye and S. Sachdev, The Effects of Coulomb Interaction on Quantum Hall Critical Points of Systems in a Periodic Potential, Phys. Rev. Lett. **80**, 5409 (1998).
[53] Jinwu Ye, The effects of weak disorders and Coulomb interaction on quantum Hall critical points, Phys. Rev. B **60**, 8290 (1999).